

Efficient Monte Carlo Methods for Cyclic Peptides

Minghong G. Wu and Michael W. Deem
Chemical Engineering Department
University of California
Los Angeles, CA 90095-1592

September 21, 2018

Abstract

We present a new, biased Monte Carlo scheme for simulating complex, cyclic peptides. Backbone atoms are equilibrated with a biased rebridging scheme, and side-chain atoms are equilibrated with a look-ahead configurational bias Monte Carlo. Parallel tempering is shown to be an important ingredient in the construction of an efficient approach.

Molecular Physics, to appear.

1 Introduction

Peptides are of fundamental importance in biological systems. They regulate homeostasis, particularly thirst, feeding and pain [1], serve as important signaling molecules in the nervous system [2], and are used as a chemical defense mechanism by some organisms [3]. Peptides have been used within the biotechnology industry to identify antagonists blocking various abnormal enzymatic reactions or ligand-receptor interactions [4]. Cyclic peptides or constrained peptides are often preferred for this application, since such molecules lose less configurational entropy upon binding [5]. Cyclic peptides have backbones with a cyclic topology that is formed either by the condensation of two sulfhydryl (-SH) groups from two cysteine side chains or by the dyhydration of the head NH_2 and tail COOH groups. A classic example of using a cyclic peptide as an antagonist is the blocking of platelet aggregation by RGD peptides. The GPIIb/IIIa-fibronectin interaction is known to be responsible for blood platelet aggregation [6]. Roughly eight cyclic peptides of the form $\overline{\text{CRGDxxxC}}$, $\overline{\text{CxxxRGDC}}$, and $\overline{\text{CxxxKGDC}}$ that are effective platelet aggregation blockers were identified [7]. Several companies are now pursuing organic analogs of these RGD peptides in clinical trials. Although no successful drug has yet been designed by purely computational methods, the discovery of the RGD peptide and roughly thirty other pharmaceuticals has benefited in some way from computer simulation [8].

Simulation of complex biomolecules with standard Metropolis Monte Carlo or conventional molecular dynamics, however, often fails to sample conformations from the correct Boltzmann distribution. The difficulty lies in the intrinsic high energy barriers between the conformations adopted at room- or body-temperature, barriers that cannot be overcome with these methods. High temperature [9] or potential-scaled [10] molecular dynamics can cross these barriers, but these methods sample from a distribution that is not the one of interest.

The configurational bias Monte Carlo method (CBMC), first developed by Frenkel, Smit, and de Pablo [11, 12], successfully samples complex energy landscapes by using local information when proposing moves. This method has been successfully applied to long chain molecules [13], phase behavior of long chain alkanes [14, 15], and conformations of hydrocarbons within zeolite channels [16]. A combination with a generalized concerted rotation scheme, inspired by the method for alkane chains [18], has been applied to the simulation of linear and cyclic peptides [17]. This approach proved to be especially efficient in sampling cyclic peptides with barrier-separated conformations, even when the location of the conformation and energy barriers were not known *a priori*. For cyclic peptides, this method changes conformations locally by perturbing backbone segments of two to three amino acids. Such moves have the potential to equilibrate large molecules with complex topologies.

Despite the successes of the configurational bias and concerted rotation scheme, difficulties still remain for complex cyclic peptides. Long or bulky side chains are not well equilibrated, for example. In some cases, the backbone of cyclic peptides is not sampled efficiently, due to the unpredictable presence of large barriers in the multidimensional torsional-angle free-energy landscape. We present an integrated methodology for simulation of cyclic peptides. Special concerns are given to optimizing and quantifying the efficiency of our method. We propose a peptide rebridging scheme, inspired by a method

proposed for polymers [19, 20, 21], and suitable for backbone equilibration of peptides. Eight torsional degrees of freedom are altered with this backbone move. Implementation of the move is reduced in all cases to the solution of a one-dimensional numerical problem. Four approaches to biasing the rebridging moves are proposed and compared. For side chain regrowth, we propose two new methods, ‘semi-look-ahead’ and ‘look-ahead’, inspired by Meirovitch’s lattice scanning method [22]. We find that both methods equilibrate side chains rapidly. We compare their efficiency and discuss optimal parameter values.

For the most complex cyclic peptides, biased Monte Carlo is still not optimally efficient. To overcome the remaining barriers to effective sampling, we add parallel tempering to our range of techniques. Parallel tempering is a rigorous Monte Carlo method, first proposed for the study of glassy systems with large free energy barriers [23]. This method has been successfully applied to spin glasses [24, 25], self-avoiding random walks [26], lattice QCD [27], linear peptides [28], and crystal structure determination [29]. In parallel tempering, we consider a set of identical systems, each at a distinct temperature. Each system is equilibrated with both updating and swapping moves. The swapping moves couple the systems in such a way that the lowest temperature system is able to escape from local energy minima without explicit knowledge of the barriers. This method achieves rigorously correct canonical sampling, and it significantly reduces the equilibration time. We show that the combination of biased Monte Carlo and parallel tempering achieves effective sampling, quickly overcoming energy barriers and approaching the Boltzmann distribution.

We define our all-atom, molecular model of peptides in Sec. 2.1. The peptide rebridging scheme is described in Sec. 2.2, where technical details are provided. This section can be skipped on a first reading, as it is simply an extension of the method in ref. [17] to include pre-screening. How biasing can be done is discussed in Sec. 2.3. In Sec. 2.4 we apply the concept of parallel tempering to our system. The ‘semi-look-ahead’ and ‘look-ahead’ methods for side chains are presented in Sec. 2.5 and Sec. 2.6, respectively. Results for the simulation of complex, cyclic peptides are given in Sec. 3, where the efficiency of our approach is demonstrated. We discuss the results in Sec. 4, and make our conclusions in Sec. 5.

2 Simulation Methods

2.1 Molecular Model

We chose to use the AMBER force field [30] with explicit atoms. Other suitable potential models are ECEPP [31] and CHARMM [32]. Dielectric theory was used to estimate solvent effects [33]. Fast coordinates such as bond lengths and bond angles were fixed at their equilibrium value. Only the biologically-relevant, torsional degrees of freedom were sampled. Nonetheless, this method can be easily generalized to flexible systems. With this assumption, a molecule is comprised of a set of so-called ‘rigid units’. Following the definition in ref. [17], a rigid unit consists of a set of atoms and bonds that form a rigid body. The relative distance between any pair of atoms within a rigid unit is constant. Adjacent rigid units are connected by a single sigma bond.

The rigid units are labeled from the head NH_2 to the tail COOH group of the peptide. Each rigid unit has exactly one incoming bond that starts from the previous unit and

ends within it. All other bonds that leave the unit are defined to be outgoing bonds. For example, a $C_\alpha H$ unit has two outgoing bonds, the first going to the residue and the second going to the next backbone unit. For unit i , we define θ_i to be the angle formed by the incoming bond and the outgoing bond to the next backbone unit. The atom that ends the incoming bond is defined to be a head atom, and the atom that starts the outgoing bond is defined to be a tail atom. We define \mathbf{r}_{ih} and \mathbf{r}_{it} to be the positions of the head and tail atoms of unit i , respectively.

Rigid units that appear in the backbone are divided into two topological types. Type A includes all rigid units with identical head and tail atoms. Type B includes the CONH amide group, which has $\theta_i = 0$. Figure 2 illustrates the geometry of these two types and the definitions of θ_{ih} and θ_{it} , which are the angles spanned by $\mathbf{r}_{it} - \mathbf{r}_{ih}$ and the incoming and outgoing bonds, respectively.

2.2 Rebridging Scheme

We display in Fig. 1 a typical cyclic peptide, $\overline{\text{CNWKRGD C}}$. Although the chemical functionality of peptides lies mostly in the freely-rotating side chains, backbone equilibration is important since the backbone serves as a scaffold for the side chains. We, therefore, use two types of biased Monte Carlo moves, chosen at random: movement of a random segment of the backbone with rigid rotation of the associated side chains and regrowth of a randomly picked side chain. Here we describe the backbone move, a peptide rebridging scheme.

The peptide rebridging scheme is inspired by the concerted rotation [18] and rebridging [19] moves for alkane chains and the extension of concerted rotation to peptides [17]. Peptide rebridging causes a local conformational change within the molecule, leaving the rest of the molecule fixed. Rebridging moves are not only suitable for cyclic peptides but also suitable for the internal parts of larger linear peptides and proteins. The main features that distinguish our rebridging scheme are the pre-screening process, more degrees of freedom per move, and more efficient biasing. We proposed five variations of rebridging moves, differing in the probabilities of choosing one of the many possible geometric solutions. They are Metropolis (MT), no Jacobian (NJ), with Jacobian (WJ), with Jacobian and old solutions (WJO), and with Jacobian and multiple rotations (WJM). Here we describe WJ. Other variations will be described in Section 2.3. Peptide rebridging is carried out in several steps:

1. Randomly select two torsional degrees of freedom that are separated by six other torsional degrees of freedom. We label the two torsional angles as ϕ_0 and ϕ_7 . The eight rigid units, including both ends, are labeled from unit 0 to unit 7. Backbone positions are denoted \mathbf{r}_{ia} , where $i = 0, \dots, 6$ and $a = h$ (head) or t (tail). Figure 3 depicts a segment that is selected to be rebridged.
2. The angles ϕ_0 and ϕ_7 are rotated, causing the rigid units between 0 and 6 to change while leaving the rigid units before 0 and after 6 unchanged. The range of rotation is within $\pm\Delta\phi_{\max}$. The two rotations break the connectivity of the molecule and provide new trial positions for \mathbf{r}_{1h} and \mathbf{r}_{5t} . We denote the new values by ϕ'_0 and ϕ'_7 .

3. Find all geometrical solutions, ϕ'_0, \dots, ϕ'_7 , that re-insert the backbone units in a valid way between rigid units 1 to 6. How we solve this geometrical problem will be described below. If no solution is found, this move is rejected. Otherwise, calculate the Rosenbluth factor, $W^{(n)}$, which is defined as

$$W^{(n)} = \sum_{i=1}^{k^{(n)}} J_i^{(n)} \exp(-\beta U_i^{(n)}) , \quad (1)$$

where $k^{(n)}$ is the number of geometrical solutions found. The Jacobian associated with the constraints for the i th solution is $J_i^{(n)}$.

4. Pick a solution from these $k^{(n)}$ solutions with probability

$$p_i = \frac{J_i^{(n)} \exp(-\beta U_i^{(n)})}{W_i^{(n)}} . \quad (2)$$

5. Solve the geometrical problem corresponding to ϕ_0 and ϕ_7 . These solutions include the old configuration ϕ_0, \dots, ϕ_7 and are used to calculate the old Rosenbluth factor

$$W^{(o)} = \sum_{i=1}^{k^{(o)}} J_i^{(o)} \exp(-\beta U_i^{(o)}) , \quad (3)$$

where $k^{(o)}$ is the number of solutions in the old geometry.

6. The attempted move is accepted with the probability

$$\text{acc}(o \rightarrow n) = \min \left(1, \frac{W^{(n)}}{W^{(o)}} \right) . \quad (4)$$

The Jacobian in eqs. (1) and (3) accounts for the fact that when we solve for the angles ϕ_1, \dots, ϕ_6 , we do not produce uniform distributions. The Jacobian is defined by

$$\begin{aligned} J \left(\begin{array}{c} \phi_1, \phi_2, \phi_3, \phi_4, \phi_5, \phi_6 \\ \mathbf{r}_{5t}, \hat{\mathbf{u}}_6, \gamma_6 \end{array} \right) &= \frac{\hat{\mathbf{u}}_6 \cdot \hat{\mathbf{e}}_3}{\det |\mathbf{B}|} \\ \mathbf{B}_{ij} &= [\hat{\mathbf{u}}_j \times (\mathbf{r}_{5t} - \mathbf{r}_{jh})]_i, \text{ if } j \leq 3, \\ &[\hat{\mathbf{u}}_j \times \hat{\mathbf{u}}_6]_{j-3}, \text{ if } j = 4, 5. \end{aligned} \quad (5)$$

Here $\hat{\mathbf{u}}_i$ is the unit vector of the i th incoming bond, and $\hat{\mathbf{e}}_3$ is a unit vector along the laboratory z -axis. The Eulerian angle γ_6 is the azimuthal angle of $\hat{\mathbf{u}}_7$ in a spherical coordinate system defined with $\hat{\mathbf{u}}_6$ as the z -axis. The angle is measured with respect to the plane defined by $\hat{\mathbf{u}}_6$ and $\hat{\mathbf{e}}_3$. It is worth mentioning that in refs. [17] and [18], the Jacobian lacked the $\hat{\mathbf{u}}_6 \cdot \hat{\mathbf{e}}_3$ term. The Jacobian should be invariant under orthogonal transformations, but the Jacobians in refs. [17] and [18] are not. Despite this, proper sampling was attained, because the omitted terms cancel in the acceptance ratio. This cancellation does not occur in rebridging, since $\hat{\mathbf{u}}_6$ is changed by the rotation of ϕ_7 . The Jacobian appears as a consequence of the end-atom constraints in the canonical partition function of a constrained or

cyclic molecule. The Jacobian is derived in Appendix A, where a careful discussion of the cyclic constraint is given as well.

The geometrical problem in rebridging is solved by seeking conserved quantities. It is conceptually helpful to imagine a break point in the segment to be regrown. The rigid units before the break point are built upon the positions of the preceding units, whereas the rigid units after the break point are built upon the positions of the following units. When \mathbf{r}_{ih} and $\mathbf{r}_{(i-1)t}$ are expressed in local coordinates of the $(i-1)$ th unit, the positions are said to be defined in ‘forward notation’. When we build up these positions from the opposite direction, the positions are said to be defined in ‘backward notation’. How we choose the break point depends on the identity of the rigid units to be regrown. Rigid units before the break point are always defined by forward notation and rigid units after the break point are always defined by backward notation. With forward notation we have $\mathbf{r}_{1t} = \mathbf{r}_{1t}(\phi_1)$, $\mathbf{r}_{2h} = \mathbf{r}_{2h}(\phi_1)$, $\mathbf{r}_{2t} = \mathbf{r}_{2t}(\phi_1, \phi_2)$, $\mathbf{r}_{3h} = \mathbf{r}_{3h}(\phi_1, \phi_2)$, and so on. With backward notation, we have $\mathbf{r}_{5h} = \mathbf{r}_{5h}(\phi_6)$, $\mathbf{r}_{4t} = \mathbf{r}_{4t}(\phi_6)$, $\mathbf{r}_{4h} = \mathbf{r}_{4h}(\phi_6, \phi_5)$, $\mathbf{r}_{3t} = \mathbf{r}_{3t}(\phi_6, \phi_5)$, and so on.

We use a variant of Flory’s local coordinate system [34]. The system was modified for units with $\theta_i = 0$ to reduce the number of variables appearing in the constraint equations. The general formulas for $\mathbf{r}_{(i+1)h}(\phi_1, \dots, \phi_i)$ and $\mathbf{r}_{it}(\phi_1, \dots, \phi_i)$ are

$$\begin{aligned}\mathbf{r}_{(i+1)h}(\phi_1, \dots, \phi_i) &= \mathbf{r}_{it}(\phi_1, \dots, \phi_i) + l_{it,(i+1)h} \mathbf{T}_i^{\text{lab}} \Lambda_i \Phi_i \\ \mathbf{r}_{it}(\phi_1, \dots, \phi_i) &= \mathbf{r}_{ih} + l_{ih,it} \mathbf{T}_i^{\text{lab}} \Lambda_{ih} \Phi_i\end{aligned}\tag{6}$$

where

$$\begin{aligned}\Lambda_i &\equiv \begin{pmatrix} \cos \theta_i & 0 & 0 \\ 0 & \sin \theta_i & 0 \\ 0 & 0 & \sin \theta_i \end{pmatrix} \\ \Lambda_{ih} &\equiv \begin{pmatrix} \cos \theta_{ih} & 0 & 0 \\ 0 & \sin \theta_{ih} & 0 \\ 0 & 0 & \sin \theta_{ih} \end{pmatrix} \\ \Phi_i &\equiv \begin{pmatrix} 1 \\ \cos \phi_i \\ \sin \phi_i \end{pmatrix}\end{aligned}\tag{7}$$

Here $l_{ia,jb}$ denotes the constant distance between \mathbf{r}_{ia} and \mathbf{r}_{jb} . We call unit i the reference unit of unit $i+1$. We use the form of eq. (6) because it explicitly isolates the terms involving the variable ϕ_i .

The labels a and b can be either h or t. This notation is dropped when the unit is an A unit. For example, $l_{1,2h}$ says unit 1 is an A unit and defines the distance between \mathbf{r}_{1h} and \mathbf{r}_{2h} . In this case we also drop the head or tail notation for vectors and write $\mathbf{r}_1 = \mathbf{r}_{1h} = \mathbf{r}_{1t}$.

The transformation from local coordinates to the laboratory coordinates in forward notation is

$$\begin{aligned}\mathbf{T}_1^{\text{lab}} &\equiv (\hat{\mathbf{u}}_1 \hat{\mathbf{v}}_1 \hat{\mathbf{w}}_1) \\ \mathbf{T}_i^{\text{lab}}(\phi_1, \dots, \phi_{i-1}) &\equiv (\hat{\mathbf{u}}_i \hat{\mathbf{v}}_i \hat{\mathbf{w}}_i) \\ &= \mathbf{T}_1^{\text{lab}} \mathbf{T}_{1\phi} \mathbf{T}_{1\theta} \mathbf{T}_{2\phi} \cdots \mathbf{T}_{(i-1)\phi} \mathbf{T}_{(i-1)\theta} \\ \mathbf{T}_{i\theta} &\equiv \begin{pmatrix} \cos \theta_i & -\sin \theta_i & 0 \\ \sin \theta_i & \cos \theta_i & 0 \\ 0 & 0 & 1 \end{pmatrix}\end{aligned}$$

$$\mathbf{T}_{i\phi} \equiv \begin{cases} \begin{pmatrix} 1 & 0 & 0 \\ 0 & \cos \phi_i & -\sin \phi_i \\ 0 & \sin \phi_i & \cos \phi_i \end{pmatrix}, & \text{if } \theta_i \neq 0 \\ \begin{pmatrix} 1 & 0 & 0 \\ 0 & 1 & 0 \\ 0 & 0 & 1 \end{pmatrix}, & \text{if } \theta_i = 0. \end{cases} \quad (8)$$

Here $\hat{\mathbf{u}}_i$, $\hat{\mathbf{v}}_i$, and $\hat{\mathbf{w}}_i$ are the axes of the local coordinates of unit i in forward notation in the laboratory frame. The last matrix is modified from Flory's coordinate system. It is defined so that $\mathbf{T}_i^{\text{lab}} = \mathbf{T}_{i-1}^{\text{lab}}$ when $\theta_i = 0$. This definition simplifies our algorithm.

For the rigid units beyond the break point, we use backward notation. In backward notation, unit $i+1$ is the reference unit of unit i . The general formulas for $\mathbf{r}_{(i-1)t}(\phi_6, \dots, \phi_{i+1})$ and $\mathbf{r}_{ih}(\phi_6, \dots, \phi_{i+1})$ are

$$\begin{aligned} \mathbf{r}_{(i-1)t}(\phi_6, \dots, \phi_{i+1}) &= \mathbf{r}_{ih}(\phi_6, \dots, \phi_{i+1}) + l_{(i-1)t,ih} \mathbf{T}_i^{\text{lab}} \Lambda_i \Phi_{i+1} \\ \mathbf{r}_{ih}(\phi_6, \dots, \phi_{i+1}) &= \mathbf{r}_{it} + l_{ih,it} \mathbf{T}_i^{\text{lab}} \Lambda_{it} \Phi_{i+1} \\ \Lambda_{it} &\equiv \begin{pmatrix} \cos \theta_{it} & 0 & 0 \\ 0 & \sin \theta_{it} & 0 \\ 0 & 0 & \sin \theta_{it} \end{pmatrix}. \end{aligned} \quad (9)$$

The transformation from local coordinates to the laboratory coordinates in backward notation is

$$\begin{aligned} \mathbf{T}_i^{\text{lab}} &\equiv (\hat{\mathbf{x}}_i \hat{\mathbf{y}}_i \hat{\mathbf{z}}_i) \\ &= \mathbf{T}_5^{\text{lab}} \mathbf{T}_{6\phi} \mathbf{T}_{5\theta} \mathbf{T}_{5\phi} \cdots \mathbf{T}_{(i+2)\phi} \mathbf{T}_{(i+1)\theta}. \end{aligned} \quad (10)$$

Here $\hat{\mathbf{x}}_i$, $\hat{\mathbf{y}}_i$, and $\hat{\mathbf{z}}_i$ are the axes of the local coordinates of unit i in backward notation in the laboratory frame.

For all rebridging cases that we consider, it is possible to find three constraint equations with three independent torsional angles and to determine the solutions by solving a one-dimensional equation numerically. The constraint equations vary depending on the types of the units 1 to 5. Table 1 lists the six distinct cases that can occur and the corresponding constraint equations. The dependencies of the backbone positions on the torsional angles are specified explicitly in the argument, and one can tell from the arguments if the positions are in forward or backward notation. Actually, cases 4 and 5 are mirror images of case 1 and 2, with the rigid units labeled in the opposite direction. Strictly speaking, then, there are only four distinct cases: cases 1, 2, 3, and 6.

In all cases, the first two constraint equations have at most two independent variables each. In one special case (case 3), an equation with only one variable is found. In the first three cases, the first two equations of each set are used to derive two torsional angles as analytic functions of ϕ_1 . These two analytic expressions are in turn substituted into the third equation, which is solved numerically in the ϕ_1 domain. In cases 1 and 2 the other two independent angles are ϕ_2 and ϕ_6 . Case 3 is special because ϕ_2 is a constant. The other torsional angle needed in the third constraint equation is ϕ_6 . In cases 4 and 5, the approach is similar, except that the equations are solved numerically in the ϕ_6 domain. In case 6, the second and fourth rigid units are arbitrary and can be either A or B. This is a special case in which \mathbf{r}_3 can be written as a function of a single, new torsional angle. This case includes, for example, ABABA, which corresponds to C_α -amide- C_α -amide- C_α . It is obvious that the geometrical constraints keep the distances $|\mathbf{r}_1 - \mathbf{r}_3|$ and $|\mathbf{r}_3 - \mathbf{r}_5|$ constant

in all possible solutions. We also know the trial distance $|\mathbf{r}_1 - \mathbf{r}_5|$ after performing the two rotations. These distances are conserved in all solutions. Therefore, possible positions of \mathbf{r}_3 should fall on the intersection of two spheres centered at \mathbf{r}_1 and \mathbf{r}_5 . Figure 4 shows the geometry of this segment and the conserved distances. If the triangle inequality

$$l_{1,3} + l_{3,5} \geq |\mathbf{r}_1 - \mathbf{r}_5|_{\text{trial}} \quad (11)$$

holds, we can define a new set of local coordinates for unit 3:

$$\begin{aligned} \hat{\mathbf{u}}'_3 &= (\mathbf{r}_5 - \mathbf{r}_1)/l_{1,5} \\ \hat{\mathbf{w}}'_3 &= \hat{\mathbf{u}}_1 \times \hat{\mathbf{u}}'_3 / |\hat{\mathbf{u}}_1 \times \hat{\mathbf{u}}'_3| \\ \hat{\mathbf{v}}'_3 &= \hat{\mathbf{w}}'_3 \times \hat{\mathbf{u}}'_3 \end{aligned} \quad (12)$$

to obtain an expression for \mathbf{r}_3 as a function of a single, new angle ϕ'_3 :

$$\mathbf{r}_3(\phi'_3) = \mathbf{r}_1 + l_{1,3} \mathbf{T}_3^{\text{lab}'} \Lambda'_3 \Phi'_3, \quad (13)$$

where

$$\begin{aligned} \mathbf{T}_3^{\text{lab}'} &\equiv (\hat{\mathbf{u}}'_3 \ \hat{\mathbf{v}}'_3 \ \hat{\mathbf{w}}'_3) \\ \Lambda'_3 &\equiv \begin{pmatrix} \cos \theta'_3 & 0 & 0 \\ 0 & \sin \theta'_3 & 0 \\ 0 & 0 & \sin \theta'_3 \end{pmatrix} \\ \theta'_3 &\equiv \left| \cos^{-1} \frac{l_{1,3}^2 + l_{1,5}^2 - l_{3,5}^2}{2l_{1,3}l_{1,5}} \right| \\ \Phi'_3 &= \begin{pmatrix} 1 \\ \cos \phi'_3 \\ \sin \phi'_3 \end{pmatrix}. \end{aligned} \quad (14)$$

All of the constraint equations in table 1 can be grouped by their functional forms into four types. The fourth column of table 1 shows the type of each constraint equation. The general functional forms of these constraint equations are listed in table 2. The first type is a quadratic function of a single variable. The other types are functions of two torsional angles. They are based on either conserved distances, as in ‘dist’, or conserved angles, as in ‘dot’ and ‘dot1’. The last column of table 2 lists the characteristic matrix, which is used in the pre-screening process and the evaluation of the third target function.

We illustrate the peptide rebridging algorithm by taking case 6 in table 1 as an example. If eq. (11) is not satisfied, the trial move is immediately rejected because of a geometrical failure. Otherwise, we go on. The first constraint equation allows us to express ϕ_1 in terms of ϕ'_3 . To do this, we rewrite the constraint equation as

$$0 = [\mathbf{r}_3(\phi'_3) - \mathbf{r}_{2h}]^\top [\mathbf{r}_3(\phi'_3) - \mathbf{r}_{2h}] - l_{2h,3}^2$$

and use eqs. (6) and eq. (13) to obtain

$$\begin{aligned} 0 &= (l_{1,3} \mathbf{T}_3^{\text{lab}'} \Lambda'_3 \Phi'_3 - l_{1,2h} \mathbf{T}_1^{\text{lab}} \Lambda_1 \Phi_1)^\top (l_{1,3} \mathbf{T}_3^{\text{lab}'} \Lambda'_3 \Phi'_3 - l_{1,2h} \mathbf{T}_1^{\text{lab}} \Lambda_1 \Phi_1) - l_{2h,3}^2 \\ &= l_{1,3}^2 + l_{1,2h}^2 - l_{2h,3}^2 - 2l_{1,3}l_{1,2h} \Phi_3'^\top \Lambda_3'^\top \mathbf{T}_3^{\text{lab}'}{}^\top \mathbf{T}_1^{\text{lab}} \Lambda_1 \Phi_1. \end{aligned} \quad (15)$$

We introduce the constant matrix

$$\mathbf{C} \equiv \begin{pmatrix} 1 & 0 & 0 \\ 0 & 0 & 0 \\ 0 & 0 & 0 \end{pmatrix} \quad (16)$$

and multiply the first three constant terms in eq. (15) by $\Phi_3'^\top \mathbf{C} \Phi_1$, which is unity, to obtain

$$\Phi_3'^\top \mathbf{M} \Phi_1 = 0, \quad (17)$$

where the constant characteristic matrix \mathbf{M} is defined as

$$\mathbf{M} = (l_{1,3}^2 + l_{1,2h}^2 - l_{2h,3}^2)\mathbf{C} - 2l_{1,3}l_{1,2h}\Lambda_3'^\top (\mathbf{T}_3^{\text{lab}'})^\top \mathbf{T}_1^{\text{lab}} \Lambda_1. \quad (18)$$

In each case, the first two constraint equations can be cast into the form of eq. (17). The right hand column of table 2 lists the constraint equations and the corresponding characteristic matrix \mathbf{M} for each case. Equation (18), for example, is a special case of the ‘dist’ type constraint equation in table 2, in which we have $\mathbf{r}_{i'} = \mathbf{r}_{j'} = \mathbf{r}_1$.

To solve the constraint equations, we set $\omega_i = \cos(\phi_i/2)$ and use

$$\begin{aligned} \cos \phi_i &= (1 - \omega_i^2)/(1 + \omega_i^2) \\ \sin \phi_i &= 2\omega_i/(1 + \omega_i^2) \end{aligned} \quad (19)$$

to replace each $\cos \phi_i$ and $\sin \phi_i$ in eq. (17). We rewrite eq. (18) as

$$\Omega_3'^\top \mathbf{M}' \Omega_1 = 0, \quad (20)$$

where

$$\Omega_i \equiv \begin{pmatrix} 1 \\ \omega_i \\ \omega_i^2 \end{pmatrix}. \quad (21)$$

The matrix \mathbf{M}' is related to \mathbf{M} by

$$\mathbf{M}' = \begin{pmatrix} M_{11} + M_{12} + M_{21} + M_{22} & 2(M_{13} + M_{23}) & M_{11} - M_{12} + M_{21} - M_{22} \\ 2(M_{31} + M_{32}) & 4M_{33} & 2(M_{31} - M_{32}) \\ M_{11} + M_{12} - M_{21} - M_{22} & 2(M_{13} - M_{23}) & M_{11} - M_{12} - M_{21} + M_{22} \end{pmatrix}. \quad (22)$$

Equation (20) is quadratic in ω_1 , and we find

$$\begin{aligned} \omega_1 &= \frac{1}{2c_2} \left[-c_1 \pm (c_1^2 - 4c_0c_2)^{\frac{1}{2}} \right] \\ &= f_{1\pm}(\omega_3'), \end{aligned} \quad (23)$$

where

$$\begin{aligned} c_0 &= M'_{11} + M'_{21}\omega_3' + M'_{31}\omega_3'^2 \\ c_1 &= M'_{12} + M'_{22}\omega_3' + M'_{32}\omega_3'^2 \\ c_2 &= M'_{13} + M'_{23}\omega_3' + M'_{33}\omega_3'^2. \end{aligned} \quad (24)$$

Since ω'_3 must produce a non-negative discriminant in eq. (23) in order to produce a real-valued ω_1 , pre-screening can be done by solving

$$c_1^2 - 4c_0c_2 = 0 . \quad (25)$$

Equation (25) is a quartic polynomial equation. We use an eigenvalue method to solve this equation and to determine the valid domains of ϕ'_3 in the first constraint equation [35]. Note that $\phi_1 = f_{1\pm}(\phi'_3)$ has two branches.

Following a derivation parallel to that in eqs. (15)–(25), we can write $\phi_6 = f_{2\pm}(\phi'_3)$. A similar pre-screening process is done to determine the valid domains of ϕ'_3 in the second equation. This pre-screening process reduces the CPU cost and increases the efficiency of the algorithm considerably.

Evaluation of the third target function is performed over the valid domains of ϕ'_3 , which are the intersections of the valid domains found by pre-screening. The independent variable is chosen to be ϕ'_3 instead of ω'_3 , since the latter may be valid on an infinite domain. To find the acceptable new rigid unit positions, the third target function is solved. To evaluate the target function, a series of calculations is repeated for each ϕ'_3 . First, we calculate the corresponding ϕ_1 and ϕ_6 . Second, we determine $\mathbf{r}_3(\phi'_3)$, $\mathbf{r}_{2h}(\phi_1)$, and $\mathbf{r}_{4t}(\phi_6)$. Third, we calculate \mathbf{r}_{2t} and \mathbf{r}_{4h} , which are uniquely determined by the trial $\mathbf{r}_3(\phi'_3)$, $\mathbf{r}_{2h}(\phi_1)$, and $\mathbf{r}_{4t}(\phi_6)$ (see figure 4). Finally, we substitute \mathbf{r}_{2t} and \mathbf{r}_{4h} into the target function. We evaluate the target function on a grid, using a grid width of 0.003 radians. A finer grid is used when the function approaches zero. The function values so obtained are used to locate approximately the roots. Brent's method is used to refine the roots [35]. The roots for ϕ'_3 are sufficient to determine all the backbone positions. Substituting each root into $f_{1\pm}$ and $f_{2\pm}$, we obtain ϕ_1 and ϕ_6 , and thus \mathbf{r}_{2h} , \mathbf{r}_{4t} , and \mathbf{r}_3 . Other backbone positions can be calculated easily. Side chains are rigidly rotated so as to connect to the backbone properly, and the geometrical problem is solved.

For each valid ϕ'_3 , there are two branches of the solution for $\phi_1 = f_{1\pm}(\phi'_3)$ and also two branches of the solution for $\phi_6 = f_{2\pm}(\phi'_3)$. Therefore, the target function has four branches. Figure 5 shows a typical target function. In the case shown in figure 5, there are six solutions.

In summary, the algorithm for solving the geometrical problem for case 6 works as follows:

1. If the geometry does not satisfy eq. (11), the move is rejected.
2. Calculate the characteristic matrices, M_1 and M_2 , of the first two constraint equations. Transform M_1 to M'_1 and M_2 to M'_2 , using eq. (22). Find the intersection of valid domains using eq. (25). If no common domain is found, the move is rejected.
3. Search for roots of the third equation on the valid ϕ'_3 domains. Determine all the backbone positions associated with each solution for ϕ'_3 . Determine the positions of all associated side chains.

Other cases in table 1 are solved similarly, except that the independent variable is either ϕ_1 or ϕ_6 .

2.3 Biasing of the Rebridging Moves

There are several ways to bias solutions in the rebridging scheme. The first method is discussed in [17]. The Rosenbluth factors are defined as

$$\begin{aligned} W^{(n)} &= \sum_{i=1}^{k^{(n)}} \exp(-\beta U_i^{(n)}) \\ W^{(o)} &= \sum_{i=1}^{k^{(o)}} \exp(-\beta U_i^{(o)}) \end{aligned} \quad (26)$$

The proposed move is accepted with the probability

$$\text{acc}(o \rightarrow n) = \min \left(1, \frac{J^{(n)} W^{(n)}}{J^{(o)} W^{(o)}} \right), \quad (27)$$

where J is the Jacobian. This method is called no Jacobian (NJ).

A second method of bias, called with Jacobian (WJ), includes the bias introduced by the Jacobian within the Rosenbluth factors, as in eqs. (1) and (3). The proposed move is accepted with the probability given by eq. (4). This approach is expected to achieve better sampling than NJ, since it explicitly includes the bias introduced by the Jacobian within the move [36].

A third method of bias includes the old and new solutions within a single Rosenbluth factor. Solutions are picked with the probability

$$\begin{aligned} p_i &= \frac{J_i \exp(-\beta U_i)}{W}, \quad i = 1, \dots, (k^{(o)} + k^{(n)}) \\ W &= W^{(o)} + W^{(n)}. \end{aligned} \quad (28)$$

Here the Rosenbluth factors are, again, defined as in eqs. (1) and (3). Such a move is always accepted, although the new state may be identical with the old state. This method is called with Jacobian and old solutions (WJO).

It is possible to perform multiple rotations on ϕ_0 and ϕ_7 . This scheme must be based on WJ or NJ so as to satisfy detailed balance. We choose WJ and call this method with Jacobian and multiple rotations (WJM). For a rebridging move with k_{\max} rotations, $k_{\max} - 1$ rotations around the old state must be performed to obtain a correct old Rosenbluth factor. A new configuration is selected from the solutions with the probability

$$p_i = \frac{J_i^{(n)} \exp(-\beta U_i^{(n)})}{\sum_{k=1}^{k_{\max}} W_k^{(n)}}, \quad (29)$$

where $W_k^{(n)}$ is the Rosenbluth factor of the k th rotation, as calculated by eq. (1). The acceptance probability is

$$\text{acc}(o \rightarrow n) = \min \left(1, \frac{\sum_{k=1}^{k_{\max}} W^{(n)}(k)}{\sum_{k'=1}^{k_{\max}} W^{(o)}(k')} \right). \quad (30)$$

The last method is based on Metropolis rules, in which a solution is picked at random without any bias, as in ref. [18]. The picking probability and acceptance criteria are

$$p_i = \frac{1}{k^{(n)}}$$

$$\text{acc}(o \rightarrow n) = \min \left[1, \frac{J^{(n)} k^{(n)} \exp(-\beta U^{(n)})}{J^{(o)} k^{(o)} \exp(-\beta U^{(o)})} \right]. \quad (31)$$

The method is called Metropolis (MT).

2.4 Parallel Tempering

The use of biasing mitigates, but does not eliminate, the various free energy barriers in cyclic peptides. Even a small cyclic peptide is, in a sense, a ‘glassy’ system due to these significant and unpredictably-located free energy barriers. To deal with this issue, we use parallel tempering [23].

In parallel tempering we consider an extended ensemble with n systems, labeled as $i = 1, \dots, n$. Each system is a copy of the original system, except that each is equilibrated at a distinct temperature, T_i , where $i = 1, \dots, n$ and $T_1 < T_2 < \dots < T_n$. The canonical partition function of this extended canonical ensemble is given by

$$Q = \prod_{i=1}^n Q_i, \quad (32)$$

where Q_i is the individual canonical partition function of the i th system. Two types of moves are performed in the ensemble. The first is a regular Monte Carlo move within a randomly chosen system. The second is a swapping move. A swapping move proposes to exchange the configurations of the two systems i and $j = i + 1$, $1 \leq i < n$. This move is accepted with the probability

$$\begin{aligned} \text{acc}[(i, j) \rightarrow (j, i)] &= \min[1, \exp(-\beta_i U_j - \beta_j U_i + \beta_i U_i + \beta_j U_j)] \\ &= \min[1, \exp(-\Delta\beta\Delta U)]. \end{aligned} \quad (33)$$

This technique forces each system to sample the Boltzmann distribution at the appropriate temperature. In our case, we are interested in the lowest temperature distribution only. The higher temperature systems are included solely to help the lowest temperature system to escape from local energy minima via the swapping moves. To achieve efficient sampling, the highest temperature should be such that no significant free energy barriers are observed. To ensure that the swapping moves are accepted, the energy histograms of adjacent systems should overlap. The sampling efficiency is modestly affected by the fraction of overlap. We arbitrarily chose to adjust the temperatures so that the probability of accepting a swapping move was roughly 0.1, and no attempt was made to optimize further these temperatures. We will show that the extra computational cost of simulating the higher temperature systems is more than compensated for by the increased sampling efficiency of the lowest temperature system.

2.5 Semi-Look-Ahead

Since the conformations of the side chains determine the biological activity of peptides, effective sampling of side chains is important. Our method is based on the side chain dihedral angle moves in ref. [17]. A finite regrowth probability is assigned to each side chain of the molecule. A side chain move proceeds by regrowing the side chain unit by unit, beginning from the bond connecting the backbone to the side chain. At each step, n_1 twigs are generated and used to calculate the new partial Rosenbluth factor. One of the twigs is selected with a probability proportional to the Boltzmann factor associated with that twig. The old configuration and $n_\alpha - 1$ random twigs are generated and used to calculate the old partial Rosenbluth factor. This procedure is repeated until the end of chain is reached. The new chain is accepted with the probability

$$\text{acc}(o \rightarrow n) = \min \left(1, \frac{W^{(n)}}{W^{(o)}} \right) , \quad (34)$$

where $W^{(n)}$ is the product of the new partial Rosenbluth factors, and $W^{(o)}$ is the product of the old partial Rosenbluth factors.

We propose a new method called semi-look-ahead (SLA) for side chain regrowth. For each torsionally-flexible bond, we define the group of atoms included in the partial Rosenbluth factor to be the maximum set of atoms whose positions are uniquely determined by choosing the trial rotation of this bond. Figure 6 sketches this new definition of atom groups and contrasts it with the one in ref. [17]. Our definition includes atoms beyond the boundary of rigid units, including the head atoms of rigid units adjacent to the current one. We expect SLA to achieve better sampling efficiency and faster equilibration than the method without look-ahead [17], due to the improved energy estimate for the biasing.

The incremental energy at each step can be split into the internal and external components [37]. With this decomposition, torsional angles are generated with a probability derived from the internal energy, and the partial Rosenbluth factors include the external energy only. In our system, only torsional energies can be put into internal energy, and these energies account for only a small fraction of the total energy. We find it most efficient to set the internal energy to zero and to include all of the energy within the external component.

2.6 Look Ahead

For long chains or chains with bulky units, a more extensive form of look-ahead may help to avoid proposing high energy configurations [22]. The idea is illustrated in figure 7. If we regrow the molecule by exploring the energy landscape only one rigid unit ahead, we will choose one configuration, as in figure 7a. If we can look ahead two rigid units at one time, we may find the high energy region associated with that configuration and choose a more likely one instead, as in figure 7b.

We proposed two methods for look-ahead. The idea is to include a contribution from the energetic surroundings of the succeeding unit within the Rosenbluth factor. The first method, look-ahead (LA), generates n_1 trial rotations of the unit to be regrown and n_2 trial rotations of the succeeding unit for each of the trial rotations of the first unit. In the second

method, we set $n_1 = n_2 = n$. We generate n configurations of the first rigid unit, with n configurations of the second unit associated to each. When regrowing the second unit, we use the n configurations already proposed during the regrowth of the first configuration. We, therefore, generate only the configurations for the third unit when regrowing the second unit. This method of look-ahead with recycled configurations is abbreviated as LARC.

We now describe the procedure for carrying out these methods. Suppose we want to cut and regrow rigid units $i = 1, \dots, N$. The following procedure describes how to generate and accept these units:

1. Generate a set of n_1 trial torsional angles $\{\phi_1(\alpha)\}$, $\alpha = 1, \dots, n_1$. Each angle is generated according to the internal potential of unit 1

$$p_1^{(n)}(\alpha) = C_1 \exp\{-\beta U_1^{\text{int}}[\phi_1(\alpha)]\}. \quad (35)$$

Denote the external energy of unit 1 at $\phi_1(\alpha)$ by $U_1^{\text{ext}}(\alpha)$.

2. For each trial $\phi_1(\alpha)$, generate a set of n_2 torsional angles $\{\phi_2(\alpha, \gamma)\}$. Each angle is generated according to the internal potential

$$p_2^{(n)}(\alpha, \gamma) = C_2 \exp\{-\beta U_2^{\text{int}}[\phi_2(\alpha, \gamma)]\}. \quad (36)$$

Denote the external energy of unit 2 at $\phi_1(\alpha)$ and $\phi_2(\alpha, \gamma)$ by $U_2^{\text{ext}}(\alpha, \gamma)$. For LA, the number n_1 can be different from n_2 . For LARC $n_1 = n_2$.

3. Define

$$w_2^{(n)}(\alpha) = \frac{\sum_{\gamma=1}^{n_2} \exp[-\beta U_2^{\text{ext}}(\alpha, \gamma)]}{n_2} \quad (37)$$

and

$$\begin{aligned} w_1^{(n)} &= \frac{\sum_{\alpha=1}^{n_1} \sum_{\gamma=1}^{n_2} \exp[-\beta U_1^{\text{ext}}(\alpha)] \exp[-\beta U_2^{\text{ext}}(\alpha, \gamma)]}{n_1 n_2} \\ &= \frac{\sum_{\alpha=1}^{n_1} \exp[-\beta U_1^{\text{ext}}(\alpha)] w_2^{(n)}(\alpha)}{n_1}. \end{aligned} \quad (38)$$

4. Pick a $\phi_1(\alpha)$ with the probability

$$q_1^{(n)}(\alpha) = \frac{\exp[-\beta U_1^{\text{ext}}(\alpha)] w_2^{(n)}(\alpha)}{w_1^{(n)}}. \quad (39)$$

To simplify the notation, we switch the labels of the chosen α th angle with the first torsional angle so that the chosen angle is first.

5. Repeat steps (1)-(4) for rigid unit 2 to unit $N-1$, except that for LARC, the n_2 twigs of unit 2 corresponding to the chosen unit 1 are recycled to be the n_1 ($n_1 = n_2$) trial configurations of unit 2, and so on.

6. For the Nth unit, which is the last unit, there is no need to look ahead, so we repeat step (1) and generate n_1 torsional angles $\{\phi_N(\alpha)\}$. Calculate

$$w_N^{(n)} \equiv \sum_{\alpha=1}^{n_1} \exp[-\beta U_N^{\text{ext}}(\alpha)] , \quad (40)$$

and pick a $\phi_N(\alpha)$ with the probability

$$q_N^{(n)}(\alpha) = \frac{\exp[-\beta U_N^{\text{ext}}(\alpha)]}{w_N^{(n)}} . \quad (41)$$

We also need to generate and calculate the old Rosenbluth weights:

1. Generate $n_1 - 1$ trial torsional angles with the probability given by eq. (35). These angles and the original angle comprise a set of torsional angles $\{\phi_1(\alpha)\}$. Let the original angle be labeled as $\phi_1(1)$.
2. For each $\phi_1(\alpha)$ other than $\phi_1(1)$, generate n_2 torsional angles $\{\phi_2(\alpha, \gamma)\}$. For the original angle $\phi_1(1)$, generate n_2 angles if the method is LA and $n_2 - 1$ angles if the method is LARC. For LARC add the original ϕ_2 to the set of angles generated and label the original angle as $\phi_2(1, 1)$. All configurations other than the original one are generated according to the probability

$$p_2^{(o)}(\alpha, \gamma) = C_2 \exp\{-\beta U_2^{\text{int}}[\phi_2(\alpha, \gamma)]\} . \quad (42)$$

Define $w_2^{(o)}(\alpha)$ and $w_1^{(o)}$ in an analogous way as $w_2^{(n)}(\alpha)$ and $w_1^{(n)}$.

3. Repeat the preceding two steps for unit 2 to N-1.
4. For the Nth unit, which is the last unit, generate a set of $n_1 - 1$ angles $\{\phi_N(\alpha)\}$ with the probability given by eq. (35) Add the original angle. Calculate $w_N^{(o)}$.

The proposed move is accepted with the probability

$$\text{acc}(o \rightarrow n) = \min\left(1, \frac{W^{(n)}}{W^{(o)}}\right) , \quad (43)$$

where the Rosenbluth factors are defined as

$$\begin{aligned} W^{(n)} &= \frac{\prod_{i=1}^N w_i^{(n)}}{\prod_{j=2}^N w_j^{(n)}(1)} \\ W^{(o)} &= \frac{\prod_{i=1}^N w_i^{(o)}}{\prod_{j=2}^N w_j^{(o)}(1)} . \end{aligned} \quad (44)$$

Note that the denominators of eq. (44) come from the bias introduced by eq. (39). In Appendix B we prove that the LA method satisfies detailed balance.

3 Results

3.1 Backbone

We first apply the rebridging scheme to the cyclic peptide $\overline{\text{CG}_6\text{C}}$. Simulation results for the five different variations of the rebridging scheme were generated. All simulations were performed on a Silicon Graphic Indigo² 195 MHz R10000 workstation. The system was equilibrated at 298 K. We used an optimized value of $\Delta\phi_{\text{max}} = 10^\circ$ in all simulations except for WJM, in which the optimal value was $\Delta\phi_{\text{max}} = 30^\circ$. A probability of 0.05 was assigned for equilibration of either of the two side chains, NH_2 and COOH . These two side short side chains are well equilibrated by the method without look-ahead, which is used in our simulations. We define the acceptance probability P_{acc} to be the ratio of accepted backbone moves to trial backbone moves. The efficiency of the Monte Carlo scheme is measured by the average displacement of the molecule per CPU time. We define $\Delta\phi_{\text{avg}}$ as the average of the absolute change of torsional angles per trial backbone move:

$$\Delta\phi_{\text{avg}} = \frac{\sum_{i=1}^{N_{\text{trial}}} \sum_{j=0}^7 |\Delta\phi_j(i)|}{N_{\text{trial}}} . \quad (45)$$

This value is a measure of the size of successful moves and the efficiency of the rebridging scheme. There is an intrinsic energy barrier for the $\text{C}_\beta\text{SSC}_\beta$ dihedral angle at $\phi_{\text{C}_\beta\text{SSC}_\beta} \simeq 180^\circ$. The magnitude of this barrier is estimated to be 5.5-6.5 Kcal·mol⁻¹ [17]. A barrier-crossing event happens whenever this angle crosses $\phi_{\text{C}_\beta\text{SSC}_\beta} = 180^\circ$. We define the barrier-crossing frequency as the total number of barrier-crossing events divided by the total number of backbone moves. Table 3 lists simulation results obtained with the five different rebridging methods.

Figure 8 shows histograms of the angles $\phi_{\text{C}_\beta\text{SSC}_\beta}$ observed in these simulations. The NJ method yields a left peak that is slightly higher than those from other methods. The MT method yields the lowest left peak. Although the histograms are similar, they did not converge to a unique distribution within our chosen simulation time. This is because barrier crossing was not frequent enough to produce accurate statistics.

To increase the sampling efficiency, we performed a parallel tempering simulation with 4 systems. The system temperatures were 298 K, 500 K, 1000 K, and 3000 K. The rebridging moves were performed using the WJ biasing method. The probabilities for proposing swapping moves, backbone moves, and side chain moves were 0.1, 0.45, and 0.45, respectively. When a swapping move was chosen, two randomly chosen adjacent systems were proposed to swap configurations. The probabilities for swapping the two pairs with lower temperatures were doubled to accelerate de-correlations. When a backbone move or a side chain move was proposed, the system was picked with a probability that updates the two lowest temperature systems twice as frequently. We do this because of the longer correlation times at lower temperatures. The simulation consisted of 160000 Monte Carlo cycles. Each cycle proposed four swapping or updating moves, chosen at random. The whole CPU time taken in this run was 48 hours. The initial 20000 cycles were discarded to avoid equilibration effects.

The swapping moves can occur with sufficient probability only if the energy histograms of adjacent systems overlap. Figure 9 shows that this condition is satisfied for our choice

of temperatures. Table 4 lists the acceptance probabilities of swapping moves in this simulation.

Figure 10 shows the distribution of the $C_\beta SSC_\beta$ angle observed in the simulation. The histogram converged to a unique distribution with very little simulation data. After 80000 cycles, the observed distribution was almost indistinguishable from the one observed at 160000 cycles. With parallel tempering, we obtain substantially better statistics in less computation time. In fact, the computation time was two-thirds of that used in the single temperature simulations in figure 8. Note that the histogram at 3000 K is essentially flat, and so at this temperature the molecule is free to cross the barrier at $\phi_{C_\beta SSC_\beta} \simeq 180^\circ$. Strong steric repulsion between hydrogen atoms connected to the adjacent C_β atoms still prevents the molecule from adopting a conformation with $\phi_{C_\beta SSC_\beta} \simeq 0^\circ$, but this does not hinder equilibration.

3.2 Side Chains

We performed simulations on the cyclic $\overline{\text{CNWKRGC}}$ molecule to test various side chain regrowth methods. This medically-relevant molecule has long and bulky side chains. Simulations were done both on a fixed backbone scaffold and on a backbone equilibrated with rebridging and parallel tempering. First, we fixed the backbone and chose side chains at random to regrow, using the method without look-ahead and the SLA method. We tested the dependence of the equilibration on the number of trial rotations n_1 . The backbone was fixed throughout this simulation. Figure 11 shows the energy as a function of CPU time during the equilibration period. Starting from a high energy configuration, the SLA method with $n_1 = 100$ or $n_1 = 10$ reaches equilibrium rapidly. The non-look-ahead method, however, had difficulty in finding low energy regions. It took the system with $n_1 = 10$ more than 50 minutes to reach low energy configurations. The system with $n_1 = 100$, however, never reached equilibrium during the simulation. Although the associated acceptance probabilities are not small, the use of $n = 100$ results in essentially non-ergodic sampling. We point out that the non-look-ahead method equilibrates the system faster with $n_1 = 1$ than with $n_1 = 10$ or $n_1 = 100$, although non-look-ahead is always slower than SLA.

Figure 11 may prompt the following question: How do we determine the optimal value for n_1 ? For short side chains, we expect that a small n_1 will work well. For longer side chains, we expect that a larger value of n_1 will help to explore the torsional space. The optimal value, therefore, will differ for each side chain.

We next performed parallel tempering simulations with five systems, using the SLA, LA, and LARC methods for side chain regrowth. The backbone moves were performed by the WJ biasing method. The system temperatures were 298 K, 450 K, 780 K, 1700 K, and 5000 K. The simulation consisted of 100000 Monte Carlo cycles, except in the cases of $n_1 = 1$ and $n_1 = 30$ for SLA and $n_1 \times n_2 = 20 \times 10$ for LA, for which the number of cycles were 200000, 200000, and 60000, respectively. Each cycle proposed five swapping or updating moves, chosen at random. The probabilities for proposing swapping moves, backbone moves, and side chain moves were 0.1, 0.45, and 0.45, respectively. When a swapping move was proposed, two adjacent systems were chosen randomly, with the probability of picking system 1, 2, 3, and 4 equal to $\frac{3}{7}$, $\frac{2}{7}$, $\frac{1}{7}$, and $\frac{1}{7}$, respectively. When an updating move, either for backbones or for side chains, was proposed, we chose system 1, 2, 3, 4, and 5 with the

probabilities $\frac{3}{8}$, $\frac{2}{8}$, $\frac{1}{8}$, $\frac{1}{8}$, and $\frac{1}{8}$, respectively. We focused on the sampling efficiencies for the tryptophan, lysine, and arginine residues. The lysine residue has a large number, 5, of rigid units. The tryptophan residue has an indole group. The arginine residue has a guanidine group. Both groups are bulky and tend to have low acceptance probabilities. For each side chain, we used the total torsional displacement per computation time, $\Delta\phi/\text{CPU}$, as an index to the efficiency. Both side chain moves and swapping moves contributed to $\Delta\phi$. We define the acceptance probability P_{acc} to be the ratio of successful moves to trial moves in a side chain. The results are summarized in table 5.

Among the four simulations with SLA, the choice $n_1 = 10$ yields the best efficiency for lysine, and $n_1 = 30$ yields the best efficiency for tryptophan and arginine. Among the four simulations with LA, the best efficiency for tryptophan is produced when $n_1 \times n_2 = 10 \times 5$. Lysine and arginine are equilibrated most efficiently with $n_1 \times n_2 = 10 \times 10$. With LARC the efficiency for tryptophan is the best when $n_1 = 5$. The efficiency for lysine is the best when $n_1 = 10$. Interestingly, arginine is so difficult to equilibrate, typically having such a low acceptance probability, that the efficiency was best with $n_1 = 15$. In general, LARC is more efficient than LA. Comparing the results from various methods, we find that tryptophan is equilibrated most efficiently by SLA, and lysine and arginine are equilibrated most efficiently by LARC.

4 Discussion

Among the five rebridging methods listed in table 3, WJO gives the highest acceptance probability, where P_{acc} in WJO is defined to be the probability of accepting a solution other than the old one. WJO also produces the highest $\Delta\phi_{\text{avg}}$. The distribution generated by WJO is the most smooth among the curves, which shows that it is efficient in sampling local conformations. However, the CPU time per move for WJO is slightly higher than that for WJ or NJ, since there is no early rejection in WJO. We performed simulations with WJM using different $\Delta\phi_{\text{max}}$ and found the optimal value to be $\Delta\phi_{\text{max}} = 30^\circ$. Simulations with $\Delta\phi_{\text{max}} < 30^\circ$ were dominated by smaller moves that lead to infrequent barrier-crossing. The computation cost per WJM move is roughly proportional to the number of trial rotations. It is seen in table 3 that each WJM move takes more than twice the time of a WJ move. Therefore, WJM is less efficient than the first three schemes in table 3. As expected, MT yields a fairly low acceptance probability. Taking the CPU cost into consideration, the efficiency of WJ is close to that of WJO. The efficiency of NJ is less than WJ and WJO. The WJM method is less efficient than the previous three schemes. The MT method is the least efficient.

Our rebridging scheme is capable of overcoming energy barriers and promoting the frequency of barrier crossing. The fourth column in table 3 lists the barrier-crossing frequency. The WJ method yields the highest barrier-crossing frequency, and WJO yields the lowest. This is due to the predominance of local moves in WJO. An accepted move in WJO can be a move that reconfigures six degrees of freedom only, which is less likely to lead to a barrier-crossing event.

Barrier-crossing is a rare event in a simulation of the $\overline{\text{CG}_6\text{C}}$ peptide. According to the potential of mean force determined by umbrella sampling, the potential at $\phi_{C_\beta\text{SS}C_\beta} = 90^\circ$ is

less than that at $\phi_{C_{\beta}SSC_{\beta}} = 270^{\circ}$ by roughly $1 \text{ Kcal}\cdot\text{mol}^{-1}$ [17]. We, therefore, expect the left peak to be substantially higher than the right one. Our results with biased rebridging moves are consistent with the potential of mean force, but the statistics are not good enough. Because steric repulsions are severe in our system, the correlation time for other degrees of freedom is also long, and these degrees of freedom also slow down the barrier-crossing. We suspect that there is a set of low energy conformations, separated by low-energy barriers, near $\phi_{C_{\beta}SSC_{\beta}} = 270^{\circ}$.

We have found that parallel tempering is an efficient and automatic means to overcome these barriers. The overlap of energy histograms guaranteed reasonable acceptance probabilities of the swapping moves. These swapping moves transfer configurations encountered at high temperatures to systems with low temperatures, thereby helping the low-temperature systems to escape from local energy minima. Such escape from local minima is important for efficient sampling, especially in glassy systems with high energy barriers. Cyclic peptides fall in this category, because of the torsional barriers and steric repulsions associated with the cyclic constraint. Our results provide additional evidence that parallel tempering is a powerful tool for studying glassy systems. Linear peptides, on the other hand, have a fairly simple free energy landscape, and so they do not benefit substantially from the parallel tempering approach [28].

For equilibration of side chains, we tested whether the inclusion of torsional interaction energy in the internal potential is effective. We find that the acceptance probability is lower and the simulation time is increased through the use of internal biasing. Presumably this is because U^{int} is only a small fraction of the total interaction energy, and so biasing the torsional angles according to this term does not lead to better sampling.

CBMC without any look-ahead does not equilibrate long or bulky side chains as well as does CBMC with look-ahead. The key difference is that without look-ahead, the head atoms of succeeding units are not included. Without look-ahead, a chosen rotation, though probably a low energy configuration for the local atoms, may implicitly put adjacent head atoms in high energy positions and thereby fail to find the lowest energy region. Using fewer twigs in the non-look-ahead method resulted in better equilibration, as shown by the results for $n_1 = 1$ in figure 11. This occurs because with $n_1 = 1$ the regrowing units have a better chance to miss the incorrectly identified low energy regions.

Increasing the number of twigs raises the acceptance probability in SLA, LA, and LARC, but at an increased CPU cost. The optimal n_1 is attained when these competing effects are balanced. We know that for rougher energy landscapes more trial rotations need to be generated. From the first row of table 5, all three residues were poorly equilibrated by SLA with $n_1 = 1$. The torsional displacement $\Delta\phi$ in this case comes mainly from the swapping moves. Equilibration is improved by using a greater n_1 , which increases the acceptance probabilities significantly. However, the acceptance probability for arginine with $n_1 = 100$ is lower than that with $n_1 = 30$. This means that improving the local sampling does not always lead to better global sampling, and this in turns implies the necessity of more significant look-ahead sampling. The arginine residue is both long, with four rigid units, and big, with a guanidine group at the end. Therefore, look-ahead is crucial to bypass high energy regions. Comparing the results for SLA with $n_1 = 10$, LA with $n_1 \times n_2 = 10 \times 10$, and LARC with $n_1 = 10$, we see both LA and LARC enhance the acceptance probabilities. The only exception is the shortest residue, tryptophan, for which LA yields a acceptance

probability slightly lower than that from SLA. Clearly, LARC is superior to LA, because LARC costs less computation time while yielding higher acceptance probabilities. For the long residues, lysine and arginine, LARC yields the highest efficiencies among these three methods. The results suggest that, for long and bulky side chains, significant look-ahead is necessary. It is not necessary to use the same regrowth method for all side chains. Indeed, the optimal approach is to use a different regrowth method for side chains of different identity. For short side chains, SLA appears to be optimal. For longer side chains, LARC is the best method to use. We believe there may be some cases in which look-ahead is the only efficient approach for equilibration. Likely cases are those where there is substantial crowding and steric overlap, such as docking of a drug or signaling molecule to a protein receptor site or binding of antigen by the hypervariable region of antibodies.

5 Conclusion

Peptide function comes primarily from the chemical functionality of the side chains atoms, although the side chains themselves are positioned by the backbone atoms. For cyclic peptides, both backbone and side chain atoms are difficult to equilibrate with standard simulation techniques. We have described a new and efficient Monte Carlo simulation method for complex cyclic peptides. The combination of biased, look-ahead Monte Carlo and parallel tempering leads to rapid and accurate sampling of the relevant room- or body-temperature conformations. Specifically, the look-ahead biasing is helpful for equilibrating long or bulky side chains, and the parallel tempering is essential for crossing torsional-angle free-energy barriers at a rapid rate. A variety of details, such as prescreening, improved Jacobian biasing, semi-look-ahead, and look-ahead, are important components of the method.

We believe that parallel tempering will prove to be a generally useful method for simulation of ‘glassy’ atomic systems with multiple, important conformations separated by large and unpredictable free energy barriers. Explicit atom models, which are more accurate but which also increase the ruggedness of the potential energy landscape, are naturally treated within this approach. We expect that application of our peptide simulation method to high-density or crowded situations, such as peptide-receptor or antibody-antigen binding events, will further demonstrate the efficiency and power of our approach.

Acknowledgments

We thank Marco Falcioni for many useful discussions. This research was supported by the National Science Foundation through grants CTS-9702403 and CHE-9705165.

A The Jacobian in the Rebridging Scheme

In the rebridging scheme, each solution should be weighted by a Jacobian to correct for the non-uniform distribution of the angles ϕ_1, \dots, ϕ_6 generated by the non-linear solution of the geometrical problem. We derive the Jacobian here from the classical partition function.

We initially consider a simple cyclic molecule with only N backbone atoms and N backbone torsional degrees of freedom. This assumption is relaxed at the end to accommodate the complicated backbone and side chain geometry of a real peptide. The momentum part of the partition function can be integrated out if we assume that the bond length and angle constraints are enforced by springs with infinite force constants. We, thus, focus on the configurational part. The configurational partition function is

$$\begin{aligned} Z &\equiv \int d\mathbf{r}^N \exp(-\beta U) \\ &= \int d\mathbf{r}^N d\mathbf{r}_{N+1} d\mathbf{r}_{N+2} d\mathbf{r}_{N+3} \delta^3(\mathbf{r}_{N+1} - \mathbf{r}_1) \delta^3(\mathbf{r}_{N+2} - \mathbf{r}_2) \delta^3(\mathbf{r}_{N+3} - \mathbf{r}_3) \exp(-\beta U), \end{aligned} \quad (46)$$

where we have introduced three vector delta functions to account for the cyclic constraint. The choice of fixed-end constraints is not unique. We will discuss an alternative form later in this section.

We start the derivation by performing a transformation from \mathbf{r}^N to \mathbf{y}^N

$$\begin{aligned} \mathbf{y}_1 &= \mathbf{r}_1 \\ \mathbf{y}_i &= \mathbf{r}_i - \mathbf{r}_{i-1}, \quad i = 2, \dots, N+3. \end{aligned} \quad (47)$$

The Jacobian of this transformation is unity. We transform again from \mathbf{y}^N to local coordinates. We define $l_i = |\mathbf{y}_i|$ and θ_i to be the angle formed by \mathbf{y}_i and \mathbf{y}_{i+1} . We transform from \mathbf{y}_2 to l_2 and $\hat{\mathbf{u}}_2$, where

$$\hat{\mathbf{u}}_2 \equiv \frac{\mathbf{y}_2}{|\mathbf{y}_2|}. \quad (48)$$

Then we transform from \mathbf{y}_3 to l_3 , θ_2 , and γ_2 , where γ_2 is the azimuthal angle of $\hat{\mathbf{u}}_3$ in a spherical coordinate system defined with $\hat{\mathbf{u}}_2$ as the z -axis. The angle is measured with respect to the plane defined by $\hat{\mathbf{u}}_2$ and $\hat{\mathbf{e}}_3$, the fixed laboratory z -axis. We further transform \mathbf{y}_i to a spherical coordinate system l_i , θ_{i-1} , and ϕ_{i-1} , $i = 4, \dots, N+3$. With this transformation, we obtain

$$\begin{aligned} Z &= \int d\mathbf{y}_1 l_2^2 dl_2 d\hat{\mathbf{u}}_2 l_3^2 dl_3 d\theta_2 \sin \theta_2 d\gamma_2 \int \prod_{i=3}^{N+2} dl_{i+1} d\theta_i d\phi_i \\ &\times \delta^3 \left(\sum_{j=2}^{N+1} \mathbf{y}_j \right) \delta^3(\mathbf{y}_{N+2} - \mathbf{y}_2) \delta^3(\mathbf{y}_{N+3} - \mathbf{y}_3) \\ &\times J \left(\frac{\mathbf{y}_4, \dots, \mathbf{y}_{N+3}}{l_4, \dots, l_{N+3}, \theta_3, \dots, \theta_{N+2}, \phi_3, \dots, \phi_{N+2}} \right) \exp(-\beta U). \end{aligned} \quad (49)$$

The Jacobian is simply $J = \prod_{i=3}^{N+2} l_{i+1}^2 \sin \theta_i$. The fast coordinates l_i and θ_i are fixed due to the strong harmonic potentials. We denote the equilibrium values of l_i and θ_i by l_i^0 and θ_i^0 , respectively. With very large spring constants, the dependence of the integrand

along these coordinates can effectively be replaced with delta functions. Therefore

$$\begin{aligned}
Z &= C''' \int d\mathbf{y}_1 l_2^2 dl_2 d\hat{\mathbf{u}}_2 l_3^2 dl_3 d\theta_2 \sin \theta_2 d\gamma_2 \delta(l_2 - l_2^0) \delta(l_3 - l_3^0) \delta(\theta_2 - \theta_2^0) \\
&\times \int \prod_{i=3}^{N+2} dl_{i+1} d\theta_i d\phi_i J(l_4, \dots, l_{N+3}, \theta_3, \dots, \theta_{N+2}) \exp(-\beta U_0) \\
&\times \delta^3 \left(\sum_{j=2}^{N+1} \mathbf{y}_j \right) \delta^3(\mathbf{y}_{N+2} - \mathbf{y}_2) \delta^3(\mathbf{y}_{N+3} - \mathbf{y}_3) \\
&\times \prod_{k=4}^N \delta(l_k - l_k^0) \prod_{k'=3}^{N-1} \delta(\theta_{k'} - \theta_{k'}^0) \delta \left(\left| \sum_{k''=2}^N \mathbf{y}_{k''} \right| - l_1^0 \right) \\
&\times \delta \left(\cos^{-1} \frac{\mathbf{y}_2 \cdot (-\sum_{i'=2}^N \mathbf{y}_{i'})}{|\mathbf{y}_2| |\sum_{i''=2}^N \mathbf{y}_{i''}|} - \theta_1^0 \right) \delta \left(\cos^{-1} \frac{\mathbf{y}_N \cdot (-\sum_{j'=2}^N \mathbf{y}_{j'})}{|\mathbf{y}_N| |\sum_{j''=2}^N \mathbf{y}_{j''}|} - \theta_N^0 \right), \quad (50)
\end{aligned}$$

where U_0 is the potential energy measured at the ground configuration of these hard coordinates. We now integrate over the hard coordinates l_i and θ_i . The Jacobian is simply a constant and can be taken out of the integral. Since the constraint $\delta^3(\sum_{i=2}^{N+1} \mathbf{y}_i)$ holds, we can replace every $-\sum_{i=2}^N \mathbf{y}_i$ with \mathbf{y}_{N+1} . Similarly, we can replace \mathbf{y}_2 with \mathbf{y}_{N+2} . Replacing the arguments in the last two delta functions with θ_{N+1} and θ_N , respectively, we obtain

$$\begin{aligned}
Z &= C'' \int d\mathbf{y}_1 d\hat{\mathbf{u}}_2 d\gamma_2 \int \prod_{i=N}^{N+2} dl_{i+1} d\theta_i d\phi_i \exp(-\beta U_0) \\
&\times \delta^3 \left(\sum_{j=2}^{N+1} \mathbf{y}_j \right) \delta^3(\mathbf{y}_{N+2} - \mathbf{y}_2) \delta^3(\mathbf{y}_{N+3} - \mathbf{y}_3) \delta(|\mathbf{y}_{N+1}| - l_1^0) \\
&\times \delta(\theta_{N+1} - \theta_1^0) \delta(\theta_N - \theta_N^0). \quad (51)
\end{aligned}$$

We use the equalities

$$\begin{aligned}
\delta^3(\mathbf{y}_{N+2} - \mathbf{y}_2) &= \delta(l_{N+2} - l_2) \delta^2(\hat{\mathbf{u}}_{N+2} - \hat{\mathbf{u}}_2) / l_{N+2}^2 \\
\delta^3(\mathbf{y}_{N+3} - \mathbf{y}_3) &= \delta(l_{N+3} - l_3) \delta^2(\hat{\mathbf{u}}_{N+3} - \hat{\mathbf{u}}_3) / l_{N+3}^2
\end{aligned}$$

to integrate over l_{N+1} , l_{N+2} , l_{N+3} , θ_N , and θ_{N+1} to obtain

$$\begin{aligned}
Z &= C' \int d\mathbf{y}_1 d\hat{\mathbf{u}}_2 d\gamma_2 \int \prod_{i=3}^{N+2} d\phi_i \int d\theta_{N+2} \exp(-\beta U_0) \\
&\times \delta^3 \left(\sum_{j=2}^{N+1} \mathbf{y}_j \right) \delta^2(\hat{\mathbf{u}}_{N+2} - \hat{\mathbf{u}}_2) \delta^2(\hat{\mathbf{u}}_{N+3} - \hat{\mathbf{u}}_3). \quad (52)
\end{aligned}$$

Note that

$$\begin{aligned}
\int d\theta_{N+2} \delta^2(\hat{\mathbf{u}}_{N+3} - \hat{\mathbf{u}}_3) &= \int d\theta_{N+2} \delta(\gamma_{N+2} - \gamma_2) \delta(\theta_{N+2} - \theta_2) / \sin \theta_2 \\
&= \delta(\gamma_{N+2} - \gamma_2) / \sin \theta_2. \quad (53)
\end{aligned}$$

where

$$\theta_2 = \left| \cos^{-1} \frac{\mathbf{y}_3 \cdot \mathbf{y}_{N+2}}{|\mathbf{y}_3| |\mathbf{y}_{N+2}|} \right|, \quad (54)$$

and γ_{N+2} and γ_2 are the azimuthal angles of $\hat{\mathbf{u}}_{N+3}$ and $\hat{\mathbf{u}}_3$ in a spherical coordinate system defined with $\hat{\mathbf{u}}_{N+2} = \hat{\mathbf{u}}_2$ as the z -axis. The angles are measured with respect to the plane defined by $\hat{\mathbf{u}}_2$ and $\hat{\mathbf{e}}_3$. Integrating over θ_{N+2} , we obtain

$$Z = C \int d\mathbf{y}_1 d\hat{\mathbf{u}}_2 d\gamma_2 \int \prod_{i=3}^{N+2} d\phi_i \times \exp(-\beta U_0) \delta^3 \left(\sum_{j=2}^{N+1} \mathbf{y}_j \right) \delta^2(\hat{\mathbf{u}}_{N+2} - \hat{\mathbf{u}}_2) \delta(\gamma_{N+2} - \gamma_2). \quad (55)$$

This is the partition function of a classical, cyclic molecule. We see that it is an integral over torsional space with delta function constraints. These constraints cause an intrinsically non-uniform distribution of every torsional angle, even in the absence of any energy of interaction. It is convenient to transform the last six torsional coordinates to the variables \mathbf{r}_{N+1} , $\hat{\mathbf{u}}_{N+2}$, and ϕ_{N+2} and to integrate over these six coordinates. Then

$$\begin{aligned} Z &= C \int d\mathbf{y}_1 d\hat{\mathbf{u}}_2 d\gamma_2 \int \prod_{i=3}^{N-4} d\phi_i \int d\mathbf{r}_{N+1} d\hat{\mathbf{u}}_{N+2} d\gamma_{N+2} \\ &\times \sum_{k=1}^{k_s} \left\{ J_k \left(\frac{\phi_{N-3}, \dots, \phi_{N+2}}{\mathbf{r}_{N+1}, \hat{\mathbf{u}}_{N+2}, \gamma_{N+2}} \right) \exp[-\beta U_0(k)] \right\} \delta^3 \left(\sum_{j=2}^{N+1} \mathbf{y}_j \right) \delta^2(\hat{\mathbf{u}}_{N+2} - \hat{\mathbf{u}}_2) \delta(\gamma_{N+2} - \gamma_2) \\ &= C \int d\mathbf{y}_1 d\hat{\mathbf{u}}_2 d\gamma_2 \int \prod_{i=3}^{N-4} d\phi_i \sum_{k=1}^{k_s} \left\{ J_k \left(\frac{\phi_{N-3} \dots \phi_{N+2}}{\mathbf{r}_{N+1}, \hat{\mathbf{u}}_{N+2}, \gamma_{N+2}} \right) \Big|_{\mathbf{r}_1, \hat{\mathbf{u}}_2, \gamma_2} \exp[-\beta U_0(k)] \right\}. \quad (56) \end{aligned}$$

The index k labels the solutions $\{\phi_{N-3}, \dots, \phi_{N+2}\}$ that satisfy the fixed-end constraints. The summation accounts for the fact that multiple solutions are possible. In the rebridging scheme, we always relabel $\phi_{N-3}, \dots, \phi_{N+2}$ as ϕ_1, \dots, ϕ_6 and $\mathbf{r}_1, \hat{\mathbf{u}}_2$, and γ_2 as $\mathbf{r}_5, \hat{\mathbf{u}}_6$, and γ_6 . From eq. (56) it is clear that each solution must be given a weight, which is the Jacobian.

The 6×6 Jacobian is actually the determinant of a 5×5 matrix, since the last torsional angle does not affect \mathbf{r}_5 or $\hat{\mathbf{u}}_6$. Therefore,

$$\frac{\partial \mathbf{r}_5}{\partial \phi_6} = \frac{\partial \hat{\mathbf{u}}_6}{\partial \phi_6} = 0.$$

We also know that

$$\frac{\partial \gamma_6}{\partial \phi_6} = 1.$$

So we obtain

$$\begin{aligned} J \left(\frac{\phi_1, \phi_2, \phi_3, \phi_4, \phi_5, \phi_6}{\mathbf{r}_5, \hat{\mathbf{u}}_6, \gamma_6} \right) &= \frac{\hat{\mathbf{u}}_6 \cdot \hat{\mathbf{e}}_3}{\det |B|} \\ B_{ij} &= [\hat{\mathbf{u}}_j \times (\mathbf{r}_5 - \mathbf{r}_j)]_i, \text{ if } j \leq 3 \\ &= [\hat{\mathbf{u}}_j \times \hat{\mathbf{u}}_6]_{j-3}, \text{ if } j = 4 \text{ or } 5. \quad (57) \end{aligned}$$

Since the Jacobian is independent of ϕ_6 , we might conjecture that it is also independent of ϕ_1 . The reason is that the Jacobian should not depend on the direction that we choose

for the labeling of the rigid units. Hoffmann and Knapp derived a 4×4 Jacobian depending only on ϕ_2, ϕ_3, ϕ_4 , and ϕ_5 for case 6 of table 1 [38]. We will show that, with suitable choice of end-constraint variables, a 4×4 matrix can be derived in all cases. The idea is to choose a set of end coordinates that are almost independent of ϕ_1 .

Integrating eq. (55) over ϕ_{N+2} , we obtain

$$Z = C \int d\mathbf{y}_1 d\hat{\mathbf{u}}_2 d\gamma_2 \int \prod_{i=3}^{N+1} d\phi_i \exp(-\beta U_0) \delta^3 \left(\sum_{j=2}^{N+1} \mathbf{y}_j \right) \delta^2(\hat{\mathbf{u}}_{N+2} - \hat{\mathbf{u}}_2). \quad (58)$$

Let $\Delta \mathbf{r} = \mathbf{r}_{N+1} - \mathbf{r}_{N-3}$ and introduce the following end coordinates

$$\begin{aligned} R &= |\Delta \mathbf{r}| \\ \theta_b &= \left| \cos^{-1} \left(\frac{\Delta \mathbf{r} \cdot \hat{\mathbf{u}}_{N-3}}{R} \right) \right| \\ \phi_b &= \text{the torsional angle of } \Delta \mathbf{r} \text{ in local coordinates of unit } N-3 \\ \theta_e &= \left| \cos^{-1} \left(\frac{\Delta \mathbf{r} \cdot \hat{\mathbf{u}}_{N+2}}{R} \right) \right| \\ \phi_e &= \text{the torsional angle defined by } \hat{\mathbf{u}}_{N-3}, \Delta \mathbf{r}, \text{ and } \hat{\mathbf{u}}_{N+2}. \end{aligned} \quad (59)$$

Note that R, θ_b, θ_e , and ϕ_e are independent of ϕ_{N-3} and that ϕ_b is linear in ϕ_{N-3} . Substituting these coordinates into eq. (58), we obtain

$$\begin{aligned} Z &= C \int d\mathbf{y}_1 d\hat{\mathbf{u}}_2 d\gamma_2 \int \prod_{i=3}^{N+1} d\phi_i \exp(-\beta U_0) \frac{1}{R^2 \sin \theta_b \sin \theta_e} \\ &\quad \times \delta(R - |\mathbf{r}_1 - \mathbf{r}_{N-3}|) \delta(\phi_b - \phi_b^0) \delta(\theta_b - \theta_b^0) \delta(\theta_e - \theta_e^0) \delta(\phi_e - \phi_e^0). \end{aligned} \quad (60)$$

Here

$$\begin{aligned} \theta_b^0 &= \left| \cos^{-1} \left(\frac{(\mathbf{r}_1 - \mathbf{r}_{N-3}) \cdot \hat{\mathbf{u}}_{N-3}}{|\mathbf{r}_1 - \mathbf{r}_{N-3}|} \right) \right| \\ \phi_b^0 &= \text{the torsional angle of } \mathbf{r}_1 - \mathbf{r}_{N-3} \text{ in local coordinates of unit } N-3 \\ \theta_e^0 &= \left| \cos^{-1} \left(\frac{(\mathbf{r}_1 - \mathbf{r}_{N-3}) \cdot \hat{\mathbf{u}}_2}{|\mathbf{r}_1 - \mathbf{r}_{N-3}|} \right) \right| \\ \phi_e^0 &= \text{the torsional angle defined by } \hat{\mathbf{u}}_{N-3}, \Delta \mathbf{r}, \text{ and } \hat{\mathbf{u}}_2. \end{aligned} \quad (61)$$

Transforming coordinates from $\phi_{N-3}, \dots, \phi_{N+1}$ to $R, \theta_b, \phi_b, \theta_e$, and ϕ_e , we obtain

$$\begin{aligned} Z &= C \int d\mathbf{y}_1 d\hat{\mathbf{u}}_2 d\gamma_2 \int \prod_{i=3}^{N-4} d\phi_i \int dR d\theta_b d\phi_b d\theta_e d\phi_e \frac{1}{R^2 \sin \theta_b \sin \theta_e} \\ &\quad \times \delta(R - |\mathbf{r}_1 - \mathbf{r}_{N-3}|) \delta(\theta_b - \theta_b^0) \delta(\phi_b - \phi_b^0) \delta(\theta_e - \theta_e^0) \delta(\phi_e - \phi_e^0) \\ &\quad \times \sum_{k=1}^{k_s} \left\{ \mathcal{J}_k \left(\frac{\phi_{N-3}, \dots, \phi_{N+1}}{R, \theta_b, \phi_b, \theta_e, \phi_e} \right) \Big|_{|\mathbf{r}_1 - \mathbf{r}_{N-3}|, \theta_b^0, \phi_b^0, \theta_e^0, \phi_e^0} \exp[-\beta U_0(k)] \right\} \\ &= C \int d\mathbf{y}_1 d\hat{\mathbf{u}}_2 d\gamma_2 \int \prod_{i=3}^{N-4} d\phi_i \frac{1}{R^2 \sin \theta_b \sin \theta_e} \\ &\quad \times \sum_{k=1}^{k_s} \left\{ \mathcal{J}_k \left(\frac{\phi_{N-3}, \dots, \phi_{N+2}}{R, \theta_b, \phi_b, \theta_e, \phi_e} \right) \Big|_{|\mathbf{r}_1 - \mathbf{r}_{N-3}|, \theta_b^0, \phi_b^0, \theta_e^0, \phi_e^0} \exp[-\beta U_0(k)] \right\}. \end{aligned} \quad (62)$$

The Jacobian can be rewritten as

$$J = \frac{1}{R^2 \sin \theta_b \sin \theta_e |\det(B'')|}, \quad (63)$$

where

$$\begin{aligned} B''_{1j} &= \frac{\partial R}{\partial \phi_{N-4+j}}, B''_{2j} = \frac{\partial \theta_b}{\partial \phi_{N-4+j}}, B''_{3j} = \frac{\partial \phi_b}{\partial \phi_{N-4+j}}, \\ B''_{4j} &= \frac{\partial \theta_e}{\partial \phi_{N-4+j}}, B''_{5j} = \frac{\partial \phi_e}{\partial \phi_{N-4+j}}, \quad j = 1, \dots, 5. \end{aligned} \quad (64)$$

The first column of B'' has only one non-zero element, which is $B''_{31} = 1$. Taking the cofactor of B'_{21} , the determinant can be replaced with that of a 4×4 matrix

$$\begin{aligned} B'_{1j} &= \frac{\partial R}{\partial \phi_{N-3+j}}, B'_{2j} = \frac{\partial \theta_b}{\partial \phi_{N-3+j}}, B'_{3j} = \frac{\partial \theta_e}{\partial \phi_{N-3+j}}, \\ B'_{4j} &= \frac{\partial \phi_e}{\partial \phi_{N-3+j}}, \quad j = 1, \dots, 4. \end{aligned} \quad (65)$$

It is easy to extend our approach to include side chains and constrained torsional angles. Following an approach parallel to eqs. (46)–(49), we obtain an integral with additional degrees of freedom contributed by side chains. These degrees of freedom are not constrained, and they can be integrated out first. Therefore, we can simply replace U with an influence functional. The final form of the Jacobian is unaffected. For peptides, rotation about the C-N bond in the amide group is governed by a large force constant. In our simulation, we constrain these torsional degrees of freedom as well. Each constrained bond adds a delta function to eq. (55). Let A be the set of ϕ_i that are constrained. Then

$$\begin{aligned} Z &= C \int d\mathbf{y}_1 d\hat{\mathbf{u}}_2 d\gamma_2 \int \prod_{i=3}^{N+2} d\phi_i \exp(-\beta U_0) \delta^3 \left(\sum_{j=2}^{N+1} \mathbf{y}_j \right) \delta^2(\hat{\mathbf{u}}_{N+2} - \hat{\mathbf{u}}_2) \delta(\gamma_{N+2} - \gamma_2) \\ &\times \prod_{k \in A} \delta(\phi_k - \phi_k^0). \end{aligned} \quad (66)$$

Let $G(l, N+2)$ denote the last l flexible torsional angles from ϕ_3 to ϕ_{N+2} . Integrating out the other degrees of freedom, we obtain

$$\begin{aligned} Z &= C \int d\mathbf{y}_1 d\hat{\mathbf{u}}_2 d\gamma_2 \int \left(\prod_{i \notin [A \cup G(6, N+2)]} d\phi_i \right) \\ &\times \sum_{k=1}^{k_s} \left\{ J_k \left(\frac{G(6, N+2)}{\mathbf{r}_{N+1}, \hat{\mathbf{u}}_{N+2}, \gamma_{N+2}} \right) \Big|_{\mathbf{r}_1, \hat{\mathbf{u}}_2, \gamma_2} \exp[-\beta U_0(k)] \right\}. \end{aligned} \quad (67)$$

If ϕ_{N+2} is constrained, \mathbf{r}_N , \mathbf{r}_{N+1} , \mathbf{r}_{N+2} , and \mathbf{r}_{N+3} define a rigid unit. The corresponding fixed-end coordinates in our algorithm are chosen to be \mathbf{r}_N , $\hat{\mathbf{u}}_{N+1}$, and γ_{N+1} , instead of \mathbf{r}_{N+1} , $\hat{\mathbf{u}}_{N+2}$, and γ_{N+2} . This apparent difference causes no ambiguity, since both sets define the same rigid unit. The Jacobian between these two sets is unity.

Relabeling the torsional angles in $G(6, N+2)$ by ϕ_1, \dots, ϕ_6 , we recover the Jacobian in eq. (5). The 4×4 Jacobian in this case can be derived analogously. The final result, which is numerically equal to eq. (5), is

$$\mathbf{J} = \frac{1}{R^2 \sin \theta_b \sin \theta_e |\det(\mathbf{B}')|}.$$

The components of \mathbf{B}' are given below:

$$\begin{aligned} \mathbf{B}'_{1j} &= \frac{\partial R}{\partial \phi_j} = \frac{1}{R} \frac{\partial \Delta \mathbf{r}}{\partial \phi_j} \cdot \Delta \mathbf{r} \\ \mathbf{B}'_{2j} &= \frac{\partial \theta_b}{\partial \phi_j} = \frac{-1}{R \sin \theta_b} \left[-\frac{1}{R} \mathbf{B}'_{1j} \Delta \mathbf{r} \cdot \hat{\mathbf{u}}_1 + \frac{\partial \Delta \mathbf{r}}{\partial \phi_j} \cdot \hat{\mathbf{u}}_1 \right] \\ \mathbf{B}'_{3j} &= \frac{\partial \theta_e}{\partial \phi_j} = \frac{-1}{R \sin \theta_e} \left[\frac{-1}{R} \mathbf{B}'_{1j} \Delta \mathbf{r} \cdot \hat{\mathbf{u}}_6 + \frac{\partial \Delta \mathbf{r}}{\partial \phi_j} \cdot \hat{\mathbf{u}}_6 + \Delta \mathbf{r} \cdot (\hat{\mathbf{u}}_j \times \hat{\mathbf{u}}_6) \right] \\ \mathbf{B}'_{4j} &= \frac{\partial \phi_b}{\partial \phi_j} \\ &= \frac{-1}{R^2 \sin \phi_e \sin \theta_b \sin \theta_e} \left\{ \frac{(\hat{\mathbf{u}}_1 \times \Delta \mathbf{r}) \cdot (\Delta \mathbf{r} \times \hat{\mathbf{u}}_6)}{R^2 \sin \phi_e \sin \theta_b \sin \theta_e} \right. \\ &\quad \times \left(2 \frac{\partial \Delta \mathbf{r}}{\partial \phi_j} \cdot \Delta \mathbf{r} \sin \theta_b \sin \theta_e + R^2 \cos \theta_b \sin \theta_e \mathbf{B}'_{2j} + R^2 \sin \theta_b \cos \theta_e \mathbf{B}'_{3j} \right) \\ &\quad \left. + \left[(\hat{\mathbf{u}}_1 \times \frac{\partial \Delta \mathbf{r}}{\partial \phi_j}) \cdot (\Delta \mathbf{r} \times \hat{\mathbf{u}}_6) + (\hat{\mathbf{u}}_1 \times \Delta \mathbf{r}) \cdot \left(\frac{\partial \Delta \mathbf{r}}{\partial \phi_j} \times \hat{\mathbf{u}}_6 + \Delta \mathbf{r} \times (\hat{\mathbf{u}}_j \times \hat{\mathbf{u}}_6) \right) \right] \right\}, \end{aligned} \tag{68}$$

where

$$\frac{\partial \Delta \mathbf{r}}{\partial \phi_j} = \hat{\mathbf{u}}_j \times (\mathbf{r}_{5t} - \mathbf{r}_{jh}).$$

The quantities needed to calculate \mathbf{B}' are $\hat{\mathbf{u}}_i$, $\Delta \mathbf{r}$, θ_b , θ_e , and $\sin \phi_e$.

B Detailed Balance for LA

In this appendix we prove that the LA method satisfies detailed balance. The proof for LARC can be done analogously and is not presented here. In our algorithm, the old Rosenbluth factor $W^{(o)}$ is not evaluated until all units have been given new positions. In fact, $W^{(o)}$ can be calculated at any time. In the proof, we calculate the partial old Rosenbluth factor $w_i^{(o)}$ of unit i once a new proposed move for unit i is made. We first derive the probability for proposing a forward move of the first unit. By analogy, we derive the probability for proposing a reverse move of the first unit. Since we generate both the old Rosenbluth factor and the new Rosenbluth factor in a random way, their probabilities should be included. This is the so-called super detailed balance condition [11]. We will show that LA satisfies super detailed balance.

Let $\alpha_1 (\text{o} \rightarrow \text{n}; \{\phi_1^{(\text{n})}(\alpha)\}, \{\phi_2^{(\text{n})}(\alpha, \gamma)\}, \{\phi_1^{(\text{o})}(\alpha')\}, \{\phi_2^{(\text{o})}(\alpha', \gamma')\})$ be the probability of proposing a move from $\phi_1^{(\text{o})}(1)$ to $\phi_1^{(\text{n})}(1)$, given $\{\phi_1^{(\text{n})}(\alpha)\}, \{\phi_2^{(\text{n})}(\alpha, \gamma)\}, \{\phi_1^{(\text{o})}(\alpha')\}$, and $\{\phi_2^{(\text{o})}(\alpha', \gamma')\}$. Consider the following three events:

1. Generating $n_1 n_2$ new twigs, which has the probability

$$\prod_{\alpha=1}^{n_1} p_1^{(\text{n})}(\alpha) \prod_{\gamma=1}^{n_2} p_2^{(\text{n})}(\alpha, \gamma) .$$

2. Picking a new twig, which has the probability $q_1^{(\text{n})}(1)$.
3. Generating $n_1 n_2$ old twigs, which has the probability is

$$\prod_{\gamma'=1}^{n_2} p_2^{(\text{o})}(1, \gamma') \prod_{\alpha'=2}^{n_1} \left(p_1^{(\text{o})}(\alpha') \prod_{\gamma'=1}^{n_2} p_2^{(\text{o})}(\alpha', \gamma') \right) .$$

The probability of the whole event, $\alpha_1 (\text{o} \rightarrow \text{n}; \{\phi_1^{(\text{n})}(\alpha)\}, \{\phi_2^{(\text{n})}(\alpha, j)\}, \{\phi_1^{(\text{o})}(\alpha')\}, \{\phi_2^{(\text{o})}(\alpha', \gamma')\})$, is the product of these three probabilities. Multiplying the three terms together, we obtain

$$\prod_{\alpha=1}^{n_1} \left(p_1^{(\text{n})}(\alpha) \prod_{\gamma=1}^{n_2} p_2^{(\text{n})}(\alpha, \gamma) \right) \times q_1^{(\text{n})}(1) \times \prod_{\gamma'=1}^{n_2} p_2^{(\text{o})}(1, \gamma') \prod_{\alpha'=2}^{n_1} \left(p_1^{(\text{o})}(\alpha') \prod_{\gamma'=1}^{n_2} p_2^{(\text{o})}(\alpha', \gamma') \right) . \quad (69)$$

Similarly, the probability of proposing the reverse move, $\alpha_1 (\text{n} \rightarrow \text{o}; \{\phi_1^{(\text{o})}(\alpha')\}, \{\phi_2^{(\text{o})}(\alpha', \gamma')\}, \{\phi_1^{(\text{n})}(\alpha)\}, \{\phi_2^{(\text{n})}(\alpha, \gamma)\})$, is

$$\prod_{\alpha'=1}^{n_1} \left(p_1^{(\text{o})}(\alpha') \prod_{\gamma'=1}^{n_2} p_2^{(\text{o})}(\alpha', \gamma') \right) \times q_1^{(\text{o})}(1) \times \prod_{\gamma=1}^{n_2} p_2^{(\text{n})}(1, \gamma) \prod_{\alpha=2}^{n_1} \left(p_1^{(\text{n})}(\alpha) \prod_{\gamma=1}^{n_2} p_2^{(\text{n})}(\alpha, \gamma) \right) . \quad (70)$$

We define U_1^{ext} as the external energy for unit 1 in the old configuration and U_1^{ext} as the external energy for unit 1 in the new configuration. Taking the ratio of eq. (69) and eq. (70), most of the probabilities for generating the twigs cancel. Replacing $q_1^{(\text{n})}(1)$ and $q_1^{(\text{o})}(1)$ with eq. (39), we obtain

$$\begin{aligned} & \frac{\alpha_1(\text{o} \rightarrow \text{n}; \{\phi_1^{(\text{n})}(\alpha)\}, \{\phi_2^{(\text{n})}(\alpha, \gamma)\}, \{\phi_1^{(\text{o})}(\alpha')\}, \{\phi_2^{(\text{o})}(\alpha', \gamma')\})}{\alpha_1(\text{n} \rightarrow \text{o}; \{\phi_1^{(\text{o})}(\alpha')\}, \{\phi_2^{(\text{o})}(\alpha', \gamma')\}, \{\phi_1^{(\text{n})}(\alpha)\}, \{\phi_2^{(\text{n})}(\alpha, \gamma)\})} \\ &= \frac{p_1^{(\text{n})}(1) \exp[-\beta U_1^{\text{ext}, \text{n}}(1)] w_2^{(\text{n})}(1) w_1^{(\text{o})}}{p_1^{(\text{o})}(1) \exp[-\beta U_1^{\text{ext}, \text{o}}(1)] w_2^{(\text{o})}(1) w_1^{(\text{n})}} \\ &= \frac{\exp(-\beta U_1^{(\text{n})}) w_2^{(\text{n})}(1) w_1^{(\text{o})}}{\exp(-\beta U_1^{(\text{o})}) w_2^{(\text{o})}(1) w_1^{(\text{n})}} , \end{aligned} \quad (71)$$

where we have used eq. (35) to obtain the last line. Similarly, we can obtain the ratio of probabilities for subsequent units. The ratio of the transition probabilities is the product

of these ratios and the ratios of the acceptance probabilities. Multiplying eq. (71) for each unit and using eqs. (43) and (44), we find that super detailed balance is satisfied:

$$\begin{aligned} \frac{\alpha(o \rightarrow n)\text{acc}(o \rightarrow n)}{\alpha(n \rightarrow o)\text{acc}(n \rightarrow o)} &= \frac{\prod_{i=1}^N \exp(-\beta U_i^{(n)})}{\prod_{i'=1}^N \exp(-\beta U_{i'}^{(o)})} \times \frac{\prod_{j=2}^N w_j^{(n)}(1) \prod_{k=1}^N w_k^{(o)}}{\prod_{j'=2}^N w_{j'}^{(o)}(1) \prod_{k'=1}^N w_{k'}^{(n)}} \frac{W^{(n)}}{W^{(o)}} \\ &= \frac{\exp(-\beta U^{(n)})}{\exp(-\beta U^{(o)})}. \end{aligned} \quad (72)$$

References

- [1] KANDEL, E., and ABEL, T., 1995, *Science*, **268**, 825.
- [2] NELSON, L. S., ROSOFF, M. L., and LI, C., 1998, *Science*, **281**, 1686.
- [3] OLIVERA, B. M., RIVIER, J., CLARK, C., RAMILO, C. A., CORPUZ, G. P., ABOGADIE, F. C., MENA, E. E., WOODWARD, S. R., HILLYARD, D. R., and CRUZ, L. J., 1990, *Science*, **249**, 257.
- [4] CLACKSON, T., and WELLS, J. A., 1994, *Trends Biotech.*, **12**, 173.
- [5] ALBERG, D. G., and SCHREIBER, S. L., 1993, *Science*, **262**, 248.
- [6] RUOSLAHTI, E., 1992, *J. Cancer*, **66**, 239.
- [7] O'NEIL, K. T., HOESS, R. H., JACKSON, S. A., RAMACHANDRAN, N., MOUSA, S. A., and DEGRADO, W. F., 1992, *Proteins: Structure, Function, and Genetics*, **14**, 509.
- [8] BOYD, D. B., 1998, in *Rational Drug Design*, edited by REEDY, M. R., and PARRILL, A. L. (Washington, DC: American Chemical Society).
- [9] BRUCCOLERI, R. E., and KARPLUS, M., 1990, *Biopolymers*, **29**, 1847.
- [10] TSHJISHITA, H., MORIGUCHI, I., and HIRONO, S., 1994, *Biophysical J.*, **66**, 1815.
- [11] FRENKEL, D., and SMIT, B., 1996, *Understanding Molecular Simulation* (San Diego: Academic Press Inc.).
- [12] DE PABLO, J. J., LASO, M., and SUTER, U. W., 1992, *J. Chem. Phys.*, **96**, 6157.
- [13] SMIT, B., 1996, *Physica Scripta*, **T66**, 80.
- [14] SMIT, B., 1996, *Fluid Phase Equilibria*, **116**, 249.
- [15] DE PABLO, J. J., 1995, *Fluid Phase Equilibria*, **104**, 195.
- [16] BATES, S. P., VAN WELL, W. J. M., and VAN SANTEN, R. A., 1996, *J. Phys. Chem.*, **100**, 17573.
- [17] DEEM, M. W., and BADER, J. S., 1996, *Mol. Phys.*, **87**, 1245.

- [18] DODD, L. R., BOONE, T. D., and THEODOROU, D. N., 1993, *Mol. Phys.*, **78**, 961.
- [19] BOONE, T. D., 1995, *Prediction of Glass-melt Behavior and Penetrant Sorption Thermodynamics in Vinyl Polymers via Molecular Simulations*, Ph.D. thesis, UC Berkeley.
- [20] PANT, P., and THEODOROU, D. N., 1995, *Macromolecules*, **18**, 7224.
- [21] MAVRANTZAS, V., BOONE, T., ZERVOPOULOU, E., and THEODOROU, D. N., 1998, *Macromolecules*, to appear.
- [22] MEIROVITCH, H., 1985, *Phys. Rev. A*, **68**, 3699.
- [23] GEYER, C. J., 1991, in *Computing Science and Statistics*, pp. 156–163, American Statistical Association.
- [24] HUKUSHIMA, K., and NEMOTO, K., June 1996, *J. Phys. Soc. Japan*, **65**, 1604.
- [25] MARINARI, E., PARISI, G., and RUIZ-LORENZO, J., 1998, in *Spin Glasses and Random Fields*, edited by YOUNG, A., volume 12 of *Directions in condensed matter physics* (Singapore: World Scientific).
- [26] TESI, M. C., JANSE VAN RENSBURG, E. J., ORLANDINI, E., and WHITTINGTON, S. G., January 1996, *J. Stat. Phys.*, **82**, 155.
- [27] BOYD, G., January 1998, *Nucl. Phys. B (Suppl.)*, **60A**, 341.
- [28] HANSMANN, U. H. E., 1997, *Chem. Phys. Lett.*, **28**, 140.
- [29] FALCIONI, M., and DEEM, M. W., 1999, *J. Chem. Phys.*, **110**, 1754.
- [30] WEINER, S. J., KOLLMAN, P. A., NGUYEN, D. T., and CASE, D. A., 1986, *J. Comput. Chem.*, **7**, 230.
- [31] KANG, Y. K., NO, K. T., and SCHERAGA, H. A., 1996, *J. Phys. Chem.*, **100**, 15588.
- [32] MACKERELL, JR., A. D., BASHFORD, D., BELLOTT, M., DUNBRACK, JR., R. L., EVANSECK, J. D., FIELD, M. J., FISCHER, S., GAO, J., GUO, H., HA, S., JOSEPH-MCCARTHY, D., KUCHNIR, L., KUCZERA, K., LAU, F. T. K., MATTOS, C., MICHNICK, S., NGO, T., NGUYEN, D. T., PRODHOM, B., REIHER, III, W. E., ROUX, B., SCHLENKRICH, M., SMITH, J. C., STOTE, R., STRAUB, J., WATANABE, M., WIÓRKIEWICZ-KUCZERA, J., YIN, D., and KARPLUS, M., 1998, *J. Phys. Chem. B*, **102**, 3586.
- [33] SMITH, P. E., PETTITT, B. M., and KARPLUS, M., 1993, *J. Phys. Chem.*, **97**, 6907.
- [34] FLORY, P. J., 1969, *Statistical Mechanics of Chain Molecules* (New York: Wiley).
- [35] PRESS, W. H., TEUKOLSKY, S. A., VETTERLING, W. T., and FLANNERY, B. P., 1992, *Numerical Recipes in C* (New York: Cambridge), 2nd edition.
- [36] ESCOBEDO, F. A., and DE PABLO, J. J., 1995, *J. Chem. Phys.*, **104**, 4788.

[37] SMIT, B., and SIEPMANN, J. I., 1994, *J. Am. Chem. Soc.*, **98**, 8442.

[38] HOFFMANN, D., and KNAPP, E. W., 1996, *Euro. Biophys. J.*, **24**, 387.

Table 1: Constraint equations and target functions. In case 6, X can stand for either A or B, and ϕ'_3 is defined by eqs. (12) and (13).

Case	Units(1-5)	Geometrical Constraints	Classification	Comments
1	AABAB	$ \mathbf{r}_4(\phi_6) - \mathbf{r}_2(\phi_1) ^2 - l_{2,4}^2 = 0$	dist	$\phi_6 = f(\phi_1)$
		$\hat{\mathbf{u}}_3(\phi_1, \phi_2) \cdot \hat{\mathbf{u}}_6 - \cos \theta_4 = 0$	dot1	$\phi_2 = f(\phi_1)$
		$ \mathbf{r}_4[\phi_6(\phi_1)] - \mathbf{r}_{3h}[\phi_2(\phi_1)] ^2 - l_{3h,4}^2 = 0$	target	$0 = f(\phi_1)$
2	AAAAB	$ \mathbf{r}_4(\phi_6) - \mathbf{r}_2(\phi_1) ^2 - l_{2,4}^2 = 0$	dist	$\phi_6 = f(\phi_1)$
		$[\mathbf{r}_{5t} - \mathbf{r}_3(\phi_1, \phi_2)] \cdot \hat{\mathbf{u}}_6 - l_{3,4} \cos \theta_4 - l_{4,5h} - l_{5h,5t} \cos \theta_{5t} = 0$	dot	$\phi_2 = f(\phi_1)$
		$ \mathbf{r}_4[\phi_6(\phi_1)] - \mathbf{r}_3[\phi_2(\phi_1)] ^2 - l_{3,4}^2 = 0$	target	$0 = f(\phi_1)$
3	BABAB	$ \mathbf{r}_4(\phi_6) - \mathbf{r}_2(\phi_1) ^2 - l_{2,4}^2 = 0$	dist	$\phi_6 = f(\phi_1)$
		$\hat{\mathbf{u}}_3(\phi_2) \cdot \hat{\mathbf{u}}_6 - \cos \theta_4 = 0$	quad	determine ϕ_2
		$ \mathbf{r}_4[\phi_6(\phi_1)] - \mathbf{r}_{3h}(\phi_1, \phi_2) ^2 - l_{3h,4}^2 = 0$	target	$0 = f(\phi_1)$
4	BABAA	$ \mathbf{r}_4(\phi_6) - \mathbf{r}_2(\phi_1) ^2 - l_{2,4}^2 = 0$	dist	$\phi_1 = f(\phi_6)$
		$\hat{\mathbf{u}}_4(\phi_6, \phi_5) \cdot \hat{\mathbf{u}}_1 - \cos \theta_2 = 0$	dot1	$\phi_5 = f(\phi_6)$
		$ \mathbf{r}_2[\phi_1(\phi_6)] - \mathbf{r}_{3t}[\phi_5(\phi_6)] ^2 - l_{2,3t}^2 = 0$	target	$0 = f(\phi_6)$
5	BAAAA	$ \mathbf{r}_4(\phi_6) - \mathbf{r}_2(\phi_1) ^2 - l_{2,4}^2 = 0$	dist	$\phi_1 = f(\phi_6)$
		$[\mathbf{r}_{1h} - \mathbf{r}_3(\phi_6, \phi_5)] \cdot \hat{\mathbf{u}}_1 + l_{2,3} \cos \theta_2 + l_{1h,1t} \cos \theta_{1h} + l_{1t,2h} = 0$	dot	$\phi_5 = f(\phi_6)$
		$ \mathbf{r}_2[\phi_1(\phi_6)] - \mathbf{r}_3[\phi_5(\phi_6)] ^2 - l_{2,3}^2 = 0$	target	$0 = f(\phi_6)$
6	AXAXA	$ \mathbf{r}_3(\phi'_3) - \mathbf{r}_{2h}(\phi_1) ^2 - l_{2h,3}^2 = 0$	dist	$\phi_1 = f(\phi'_3)$
		$ \mathbf{r}_3(\phi'_3) - \mathbf{r}_{4t}(\phi_6) ^2 - l_{3,4t}^2 = 0$	dist	$\phi_6 = f(\phi'_3)$
		$ \mathbf{r}_{2t}[\phi_1(\phi'_3), \phi'_3] - \mathbf{r}_{4h}[\phi_6(\phi'_3), \phi'_3] ^2 - l_{2t,4h}^2 = 0$	target	$0 = f(\phi'_3)$

Table 2: The mathematical form of the constraint functions. Here i, j , and k are labels to units, and d is a constant that varies from case to case. The reference units of i and j are i' and j' , respectively. The reference unit of j' is j'' . The labels a and b are either h or t, depending on whether the notation is forward or backward. We define $a^* = \text{h}$ when $a = \text{t}$, and $a^* = \text{t}$ when $a = \text{h}$. The torsional variables that appear in the constraint equations are ϕ_{I} and ϕ_{II} . The constant characteristic matrix is \mathbf{M} . The last row defines notation used in this table. Notation not defined here is defined in Sec. 2.2.

Type	General function form	\mathbf{M} (used in $\Phi_{\text{I}}\mathbf{M}\Phi_{\text{II}} = 0$)
quad	$\hat{\mathbf{u}}_i(\phi_{\text{I}}) \cdot \hat{\mathbf{u}}_j - d = 0$	not applicable
dist	$ \mathbf{r}_{ia}(\phi_{\text{I}}) - \mathbf{r}_{jb}(\phi_{\text{II}}) ^2 - d = 0$	$(\mathbf{r}_{i'a} - \mathbf{r}_{j'b} ^2 + l_{i'a,ia}^2 + l_{j'b,jb}^2 - d)\mathbf{C}$ $- 2\mathbf{L}_{i'a}^{\text{T}}\mathbf{T}_{i'}^{\text{lab}}\mathbf{T}_{j'}^{\text{lab}}\mathbf{L}_{j'b} + 2\mathbf{L}_{i'a}^{\text{T}}\mathbf{T}_{i'}^{\text{lab}}\mathbf{T}_{j''}^{\text{lab}}\mathbf{T}_{j''}^{\text{lab}}\mathbf{L}_{j'b}$ $- 2[\Gamma(\mathbf{r}_{i'a} - \mathbf{r}_{j'b})]^{\text{T}}\mathbf{T}_{j'}^{\text{lab}}\mathbf{L}_{j'b}$
dot	$[\mathbf{r}_{ia} - \mathbf{r}_{jb}(\phi_{\text{I}}, \phi_{\text{II}})] \cdot \hat{\mathbf{u}}_k - d = 0$	$[(\mathbf{r}_{ia} - \mathbf{r}_{j''b}) \cdot \hat{\mathbf{u}}_k - d]\mathbf{C} - \mathbf{L}_{j''b}^{\text{T}}\mathbf{T}_{j''}^{\text{lab}}\mathbf{T}_{j''}^{\text{lab}}\mathbf{L}_{j''b}$ $- \mathbf{G}_{j''}(\hat{\mathbf{u}}_k)\mathbf{T}_{j''\theta}^{\text{lab}}\mathbf{L}_{j''b}$
dot1	$\hat{\mathbf{u}}_j(\phi_{\text{I}}, \phi_{\text{II}}) \cdot \hat{\mathbf{u}}_k - d = 0$	$-d\mathbf{C} + \mathbf{G}_{j''}(\hat{\mathbf{u}}_k)\mathbf{T}_{j''\theta}^{\text{lab}}\mathbf{L}_{j''b}$
\mathbf{C}	$\equiv \begin{pmatrix} 1 & 0 & 0 \\ 0 & 0 & 0 \\ 0 & 0 & 0 \end{pmatrix}$, $\Gamma(\mathbf{x}) \equiv \begin{pmatrix} \mathbf{x}_x & 0 & 0 \\ \mathbf{x}_y & 0 & 0 \\ \mathbf{x}_z & 0 & 0 \end{pmatrix}$	
$\mathbf{G}_i(\mathbf{x})$	$\equiv \begin{cases} \begin{pmatrix} [\mathbf{T}_i^{\text{lab}}\mathbf{x}]_x & 0 & 0 \\ 0 & [\mathbf{T}_i^{\text{lab}}\mathbf{x}]_y & [\mathbf{T}_i^{\text{lab}}\mathbf{x}]_z \\ 0 & [\mathbf{T}_i^{\text{lab}}\mathbf{x}]_z & -[\mathbf{T}_i^{\text{lab}}\mathbf{x}]_y \end{pmatrix}, & \text{if } \theta_i \neq 0 \\ [\Gamma(\mathbf{x})]^{\text{T}}\mathbf{T}_i^{\text{lab}} & , & \text{if } \theta_i = 0 \end{cases}$	
$\mathbf{L}_{i'a}$	$\equiv l_{i'h,i't}\Lambda_{i'a} + l_{i'a^*,ia}\Lambda_{i'}$	
$l_{i'a,ia}^2$	$\equiv l_{i'h,it}^2 + l_{i'a^*,ia}^2 + 2l_{i'h,i't}l_{i'a^*,ia}\cos\theta_{i'}$	

Table 3: Comparison of simulation results with different rebridging methods at 298 K. For all simulations $\Delta\phi_{\text{max}} = 10^\circ$, except for WJM, in which $\Delta\phi_{\text{max}} = 30^\circ$.

Method	$\Delta\phi_{\text{avg}}$ (deg)	P_{acc}	P_{cross}	Number of steps	CPU time (hrs)
NJ	6.662	0.162	0.000303	4×10^5	32
WJ	7.291	0.172	0.000414	4×10^5	32
WJO	10.006	0.177	0.000167	4×10^5	34
WJM	8.525	0.111	0.000468	2×10^5	40
MT	2.699	0.051	0.000222	4×10^5	30

Table 4: Acceptance probability observed for swapping moves in the parallel tempering simulation.

Swap	P_{acc}
298 K \leftrightarrow 500 K	0.147
500 K \leftrightarrow 1000 K	0.113
1000 K \leftrightarrow 3000 K	0.136

Table 5: Simulation data for tryptophan, lysine, and arginine residues of the $\overline{\text{CNWKRGD}}\text{C}$ peptide.

Method	$n_1 \times n_2$	Residue	$\Delta\phi/\text{CPU}$ (deg·min ⁻¹)	P_{acc}	CPU (min)
SLA	1×0	Trp	142	0.0317	2940
		Lys	82	0.00229	
		Arg	90	0.00150	
SLA	10×0	Trp	158	0.0846	1620
		Lys	575	0.187	
		Arg	152	0.0325	
SLA	30×0	Trp	315	0.313	3910
		Lys	526	0.214	
		Arg	290	0.131	
SLA	100×0	Trp	153	0.373	3220
		Lys	445	0.304	
		Arg	130	0.0821	
LA	5×5	Trp	131	0.0660	2040
		Lys	271	0.0947	
		Arg	157	0.0529	
LA	10×5	Trp	147	0.0686	2260
		Lys	375	0.169	
		Arg	205	0.0792	
LA	10×10	Trp	120	0.0841	2800
		Lys	397	0.220	
		Arg	225	0.118	
LA	20×10	Trp	28	0.120	2500
		Lys	355	0.348	
		Arg	55	0.0811	
LARC	5×5	Trp	213	0.116	1690
		Lys	673	0.221	
		Arg	327	0.100	
LARC	10×10	Trp	211	0.206	2560
		Lys	749	0.421	
		Arg	248	0.146	
LARC	15×15	Trp	151	0.334	4250
		Lys	548	0.497	
		Arg	346	0.357	
LARC	20×20	Trp	104	0.415	6420
		Lys	394	0.571	
		Arg	212	0.350	

Figure 1: A typical cyclic peptide, $\overline{\text{CNWKRGDG}}$. The disulfide bond is shown at the left, spanned by two (spherical) sulfur atoms. Note that this is not the lowest free energy conformation of this molecule.

Figure 2: Sketches for units of class A and B. The angle θ is zero for class B. Only backbone atoms are depicted here. Bold lines indicates bonds that do not rotate.

Figure 3: A segment selected to be rebridged. Change of driver angles ϕ_0 and ϕ_7 breaks the connectivity. The dotted area represents the region in which the positions of the backbone atoms must be restored.

Figure 4: The rebridging method applied to an ABABA segment. It can be seen that $|\mathbf{r}_1 - \mathbf{r}_3|$ and $|\mathbf{r}_3 - \mathbf{r}_5|$ are constants. The dotted area represents the region in which the positions of backbone atoms are to be restored.

Figure 5: A typical target function. Only the ϕ'_3 domain where the target function exists is shown here. The number of branches is four.

Figure 6: Shown as solid is the definition of atom groups used for side chain regrowth: a) in non-look-ahead and b) in semi-look-ahead. The left two bonds are connected to other rigid units.

Figure 7: Schematic pictures for generating trial moves. The solid circle 0 denotes an existing unit. Dotted circles represent trial configurations of the next unit. a) CBMC without look-ahead generates and regrows one unit at one time. Configuration 2 has the lowest energy and is most likely to be picked. b) In look-ahead, we generate two units and regrow one unit. The configurations generated from 2 turn out to be disfavored, and configuration 4 is chosen instead.

Figure 8: The probability distribution for the $C_\beta\text{SSC}_\beta$ disulfide torsional angle observed in NJ, WJ, WJO, WJM, and MT.

Figure 9: The energy histograms for all the systems in the parallel tempering simulation.

Figure 10: The histograms for the $C_\beta\text{SSC}_\beta$ disulfide torsional angle observed in the parallel tempering simulation. The total number of Monte Carlo cycles is N . The distribution at 3000 K is shown for comparison.

Figure 11: Equilibration of the side chains of $\overline{\text{CNWKRGDG}}$. The numbers at the upper right are the values of n_1 .

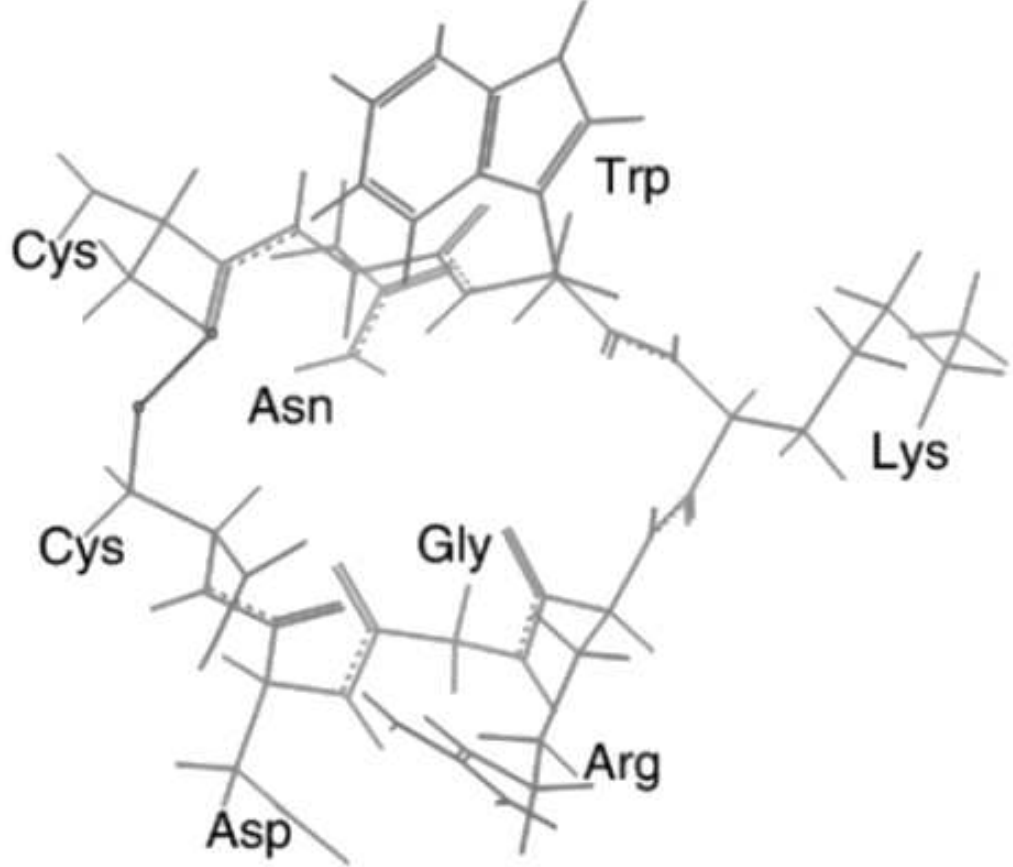


Figure 1: Wu and Deem, 'Efficient Monte Carlo...'

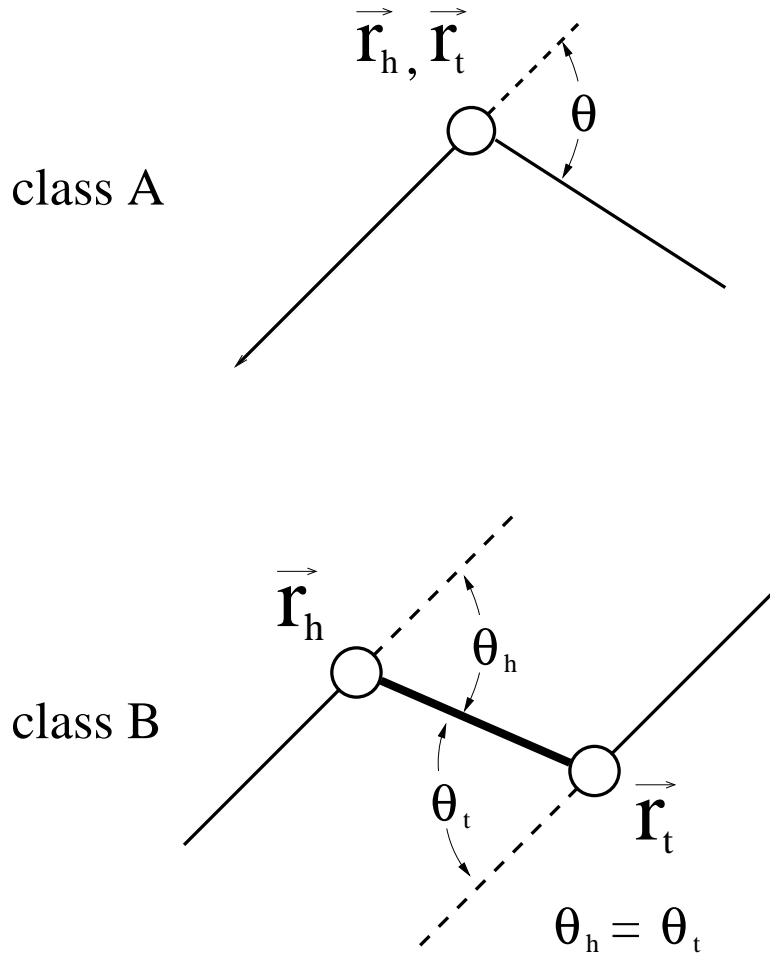


Figure 2: Wu and Deem, ‘Efficient Monte Carlo...’

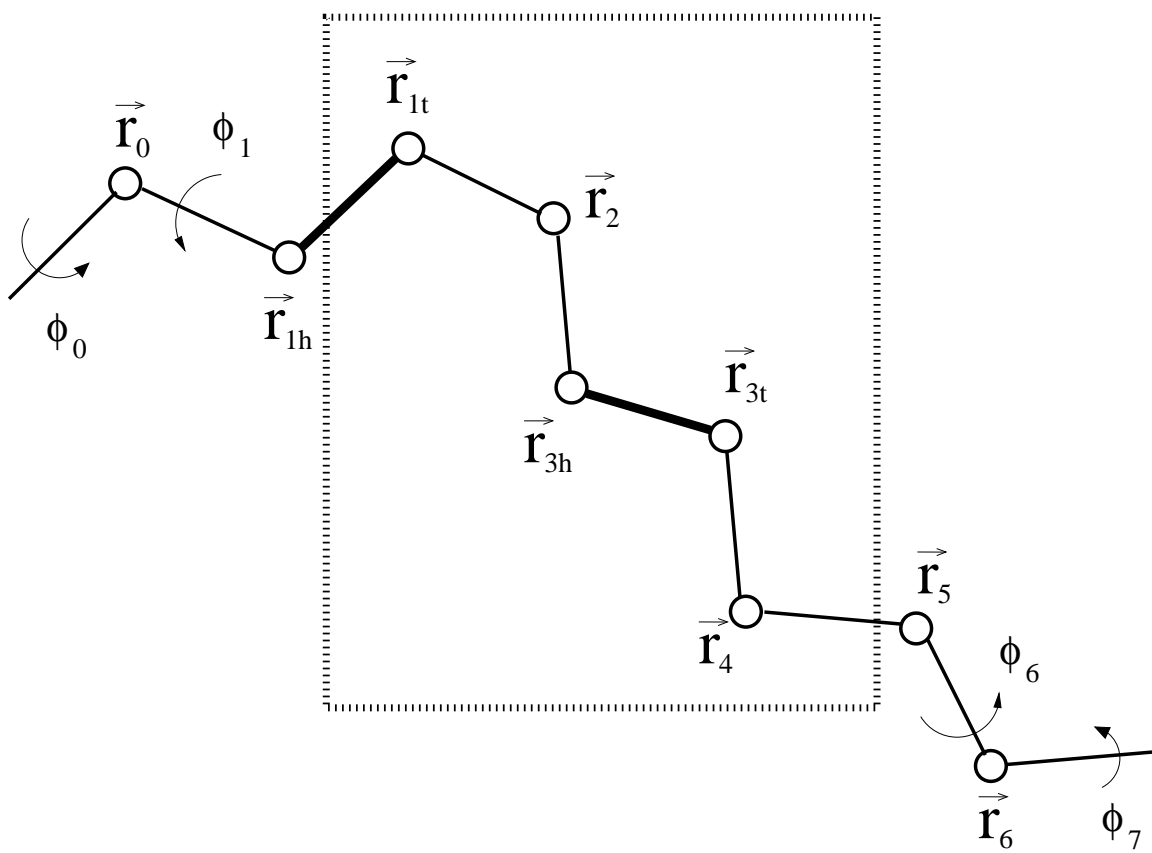


Figure 3: Wu and Deem, 'Efficient Monte Carlo...'

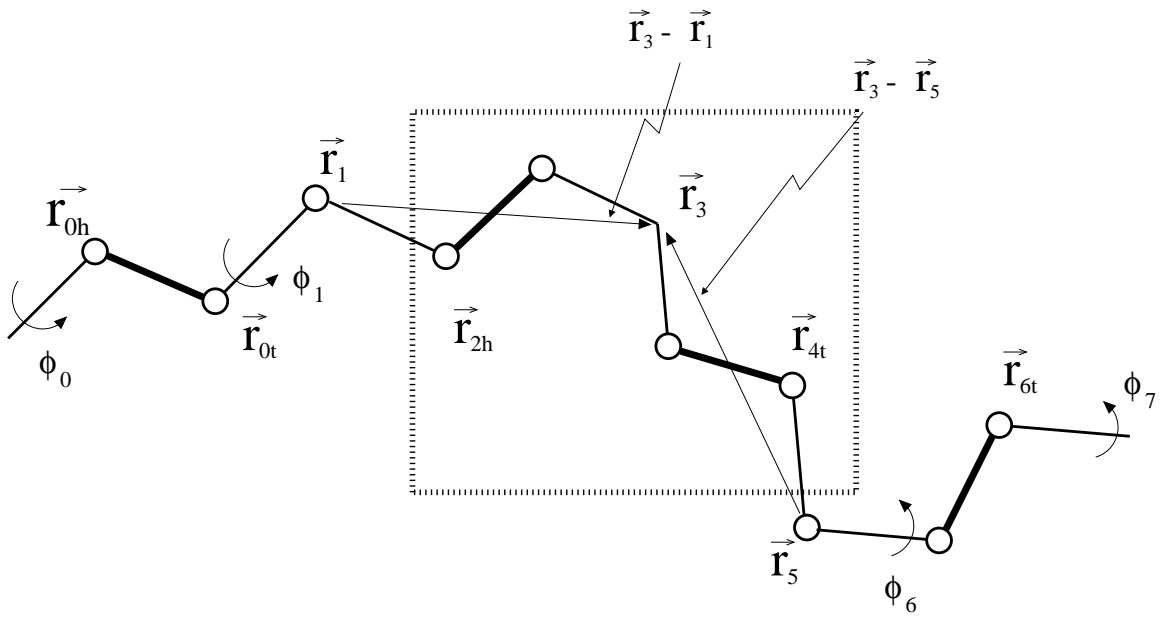


Figure 4: Wu and Deem, 'Efficient Monte Carlo...'

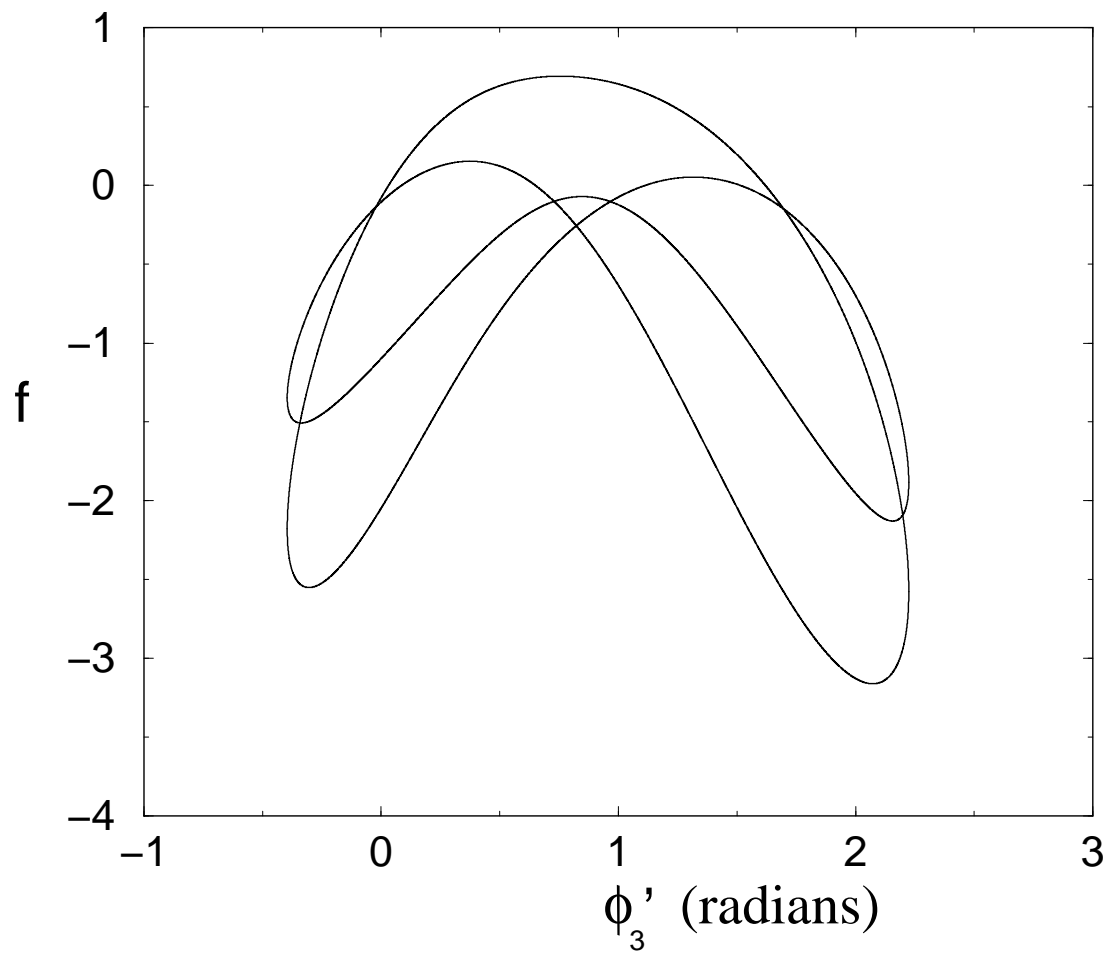


Figure 5: Wu and Deem, 'Efficient Monte Carlo...'

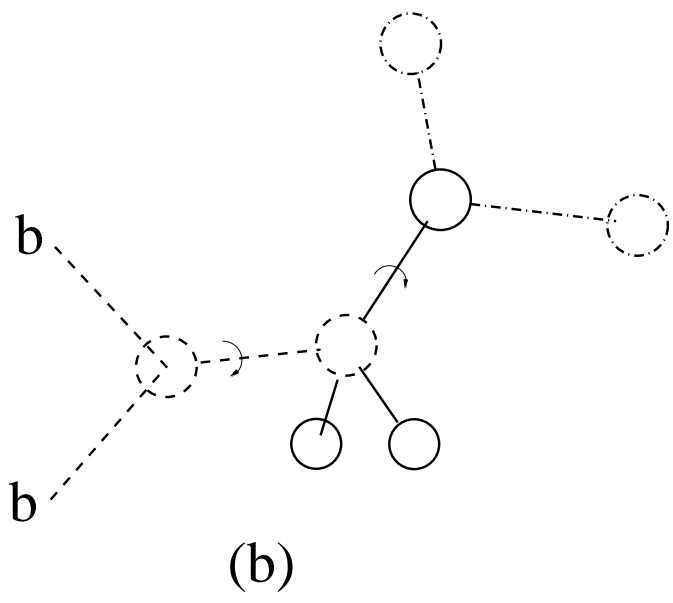
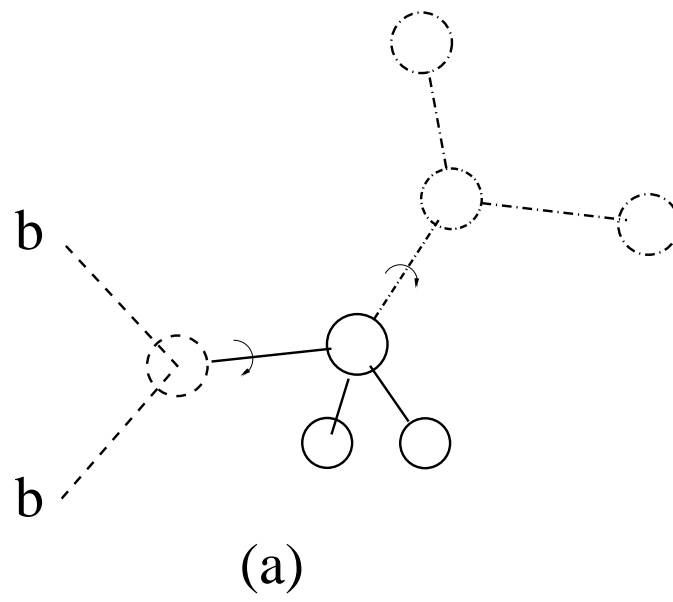


Figure 6: Wu and Deem, 'Efficient Monte Carlo...'

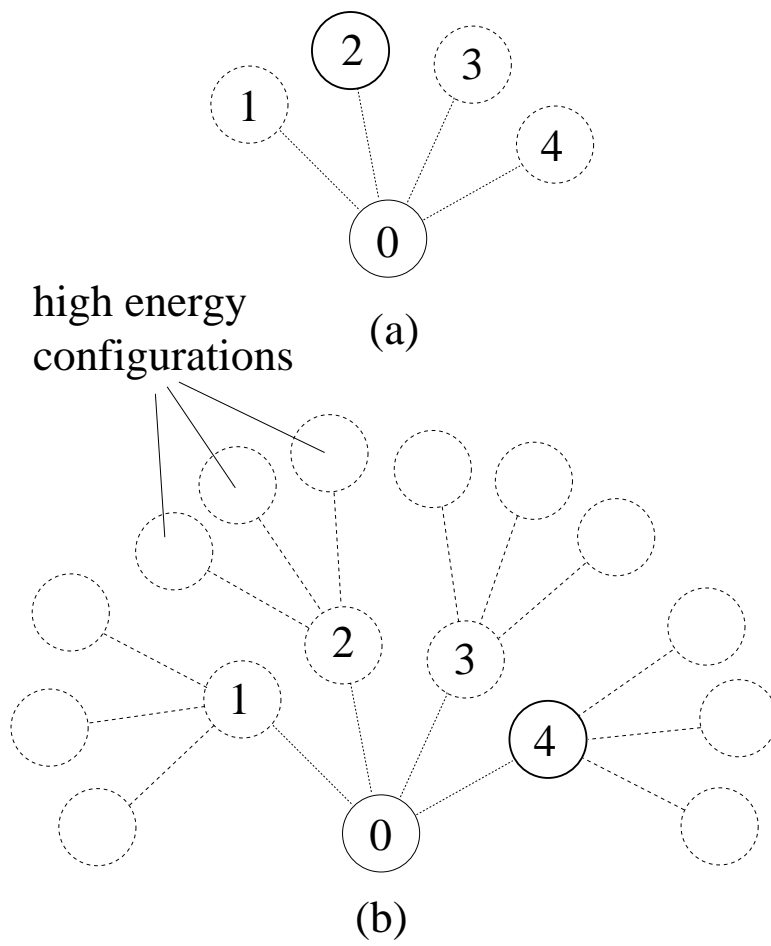


Figure 7: Wu and Deem, 'Efficient Monte Carlo...'

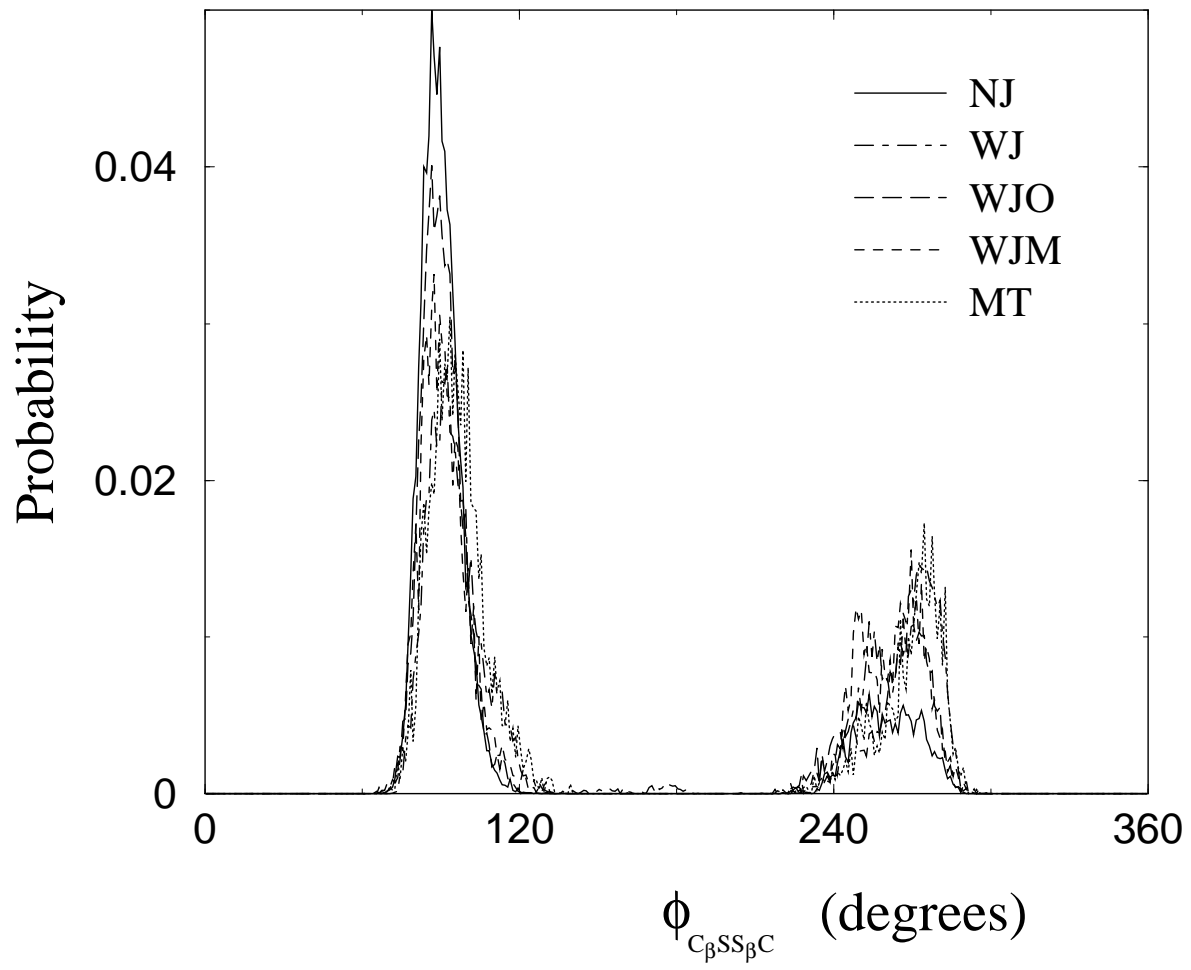


Figure 8: Wu and Deem, 'Efficient Monte Carlo...'

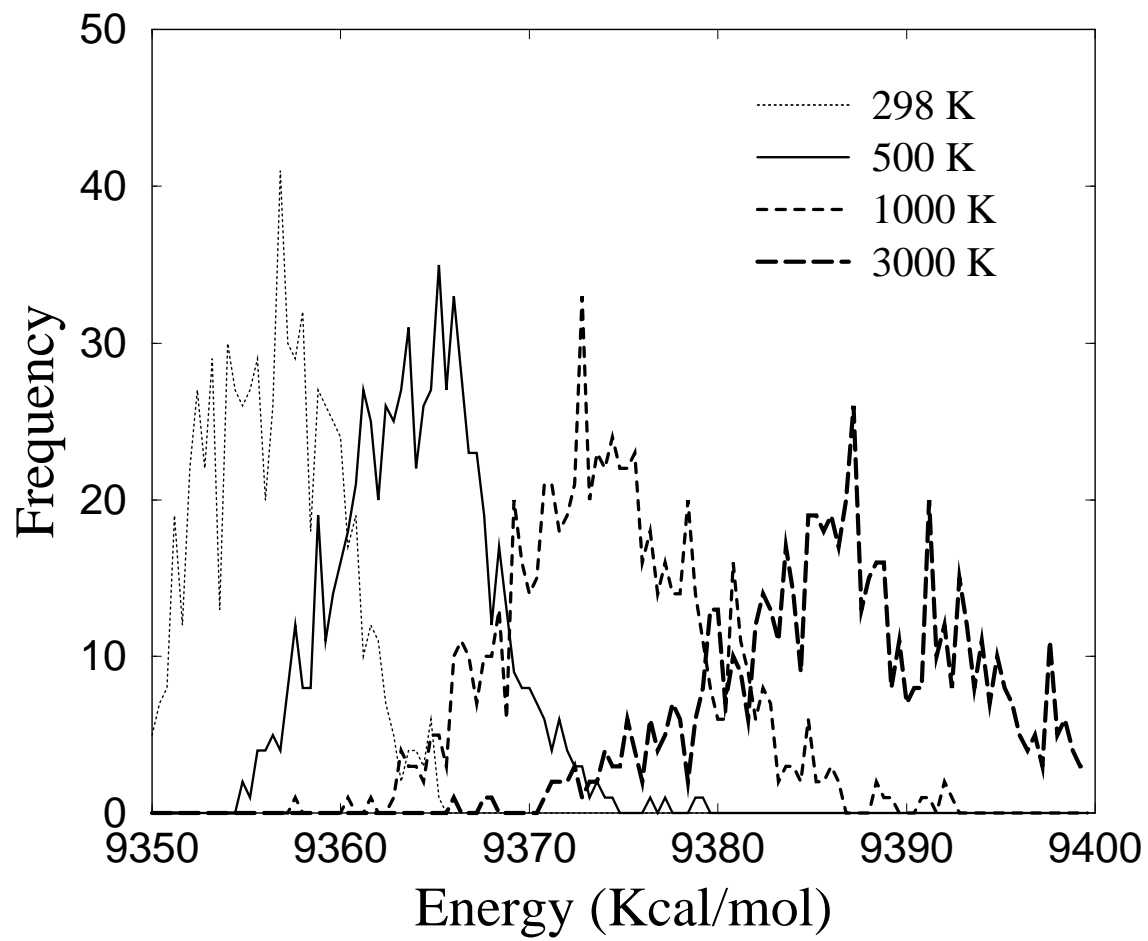


Figure 9: Wu and Deem, 'Efficient Monte Carlo...'

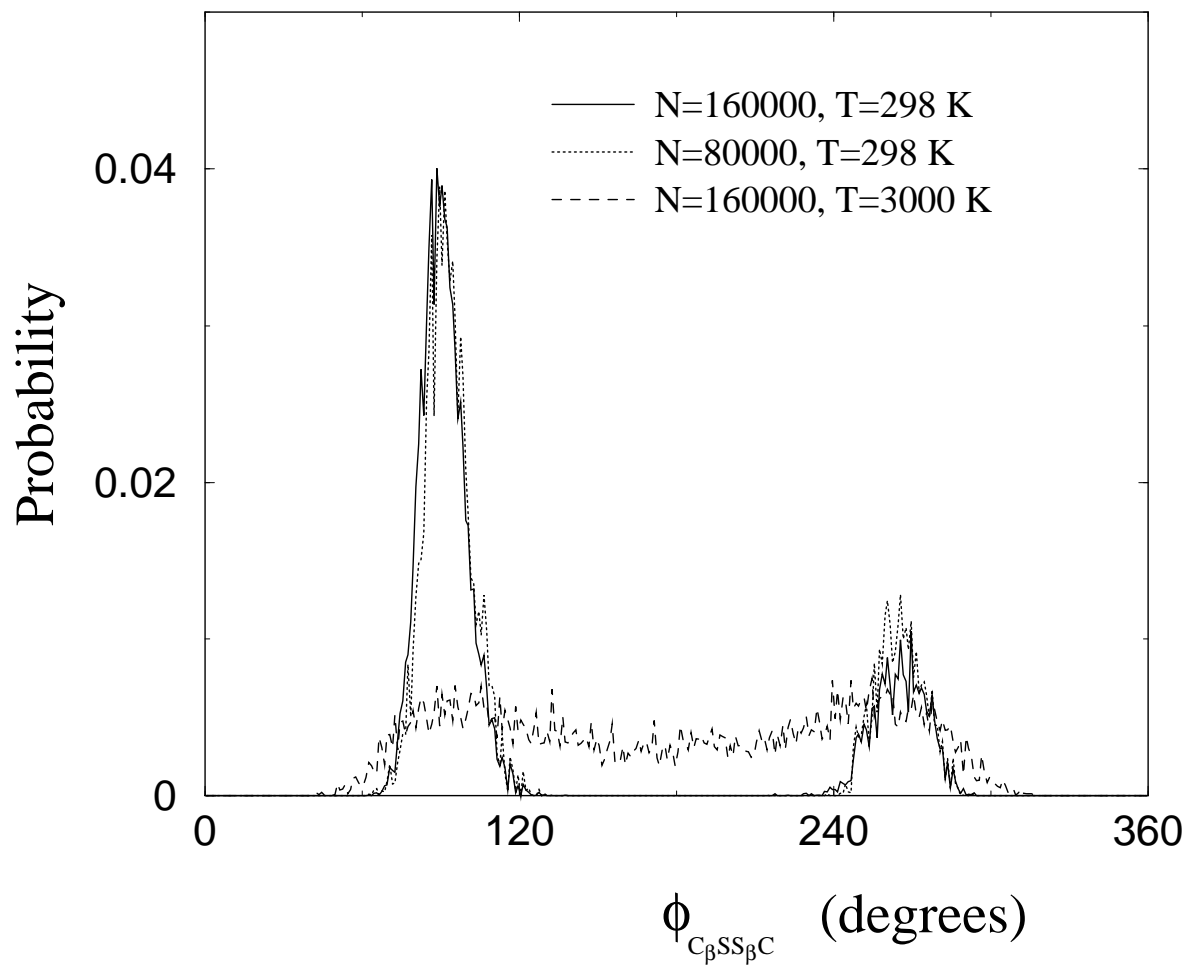


Figure 10: Wu and Deem, 'Efficient Monte Carlo...'

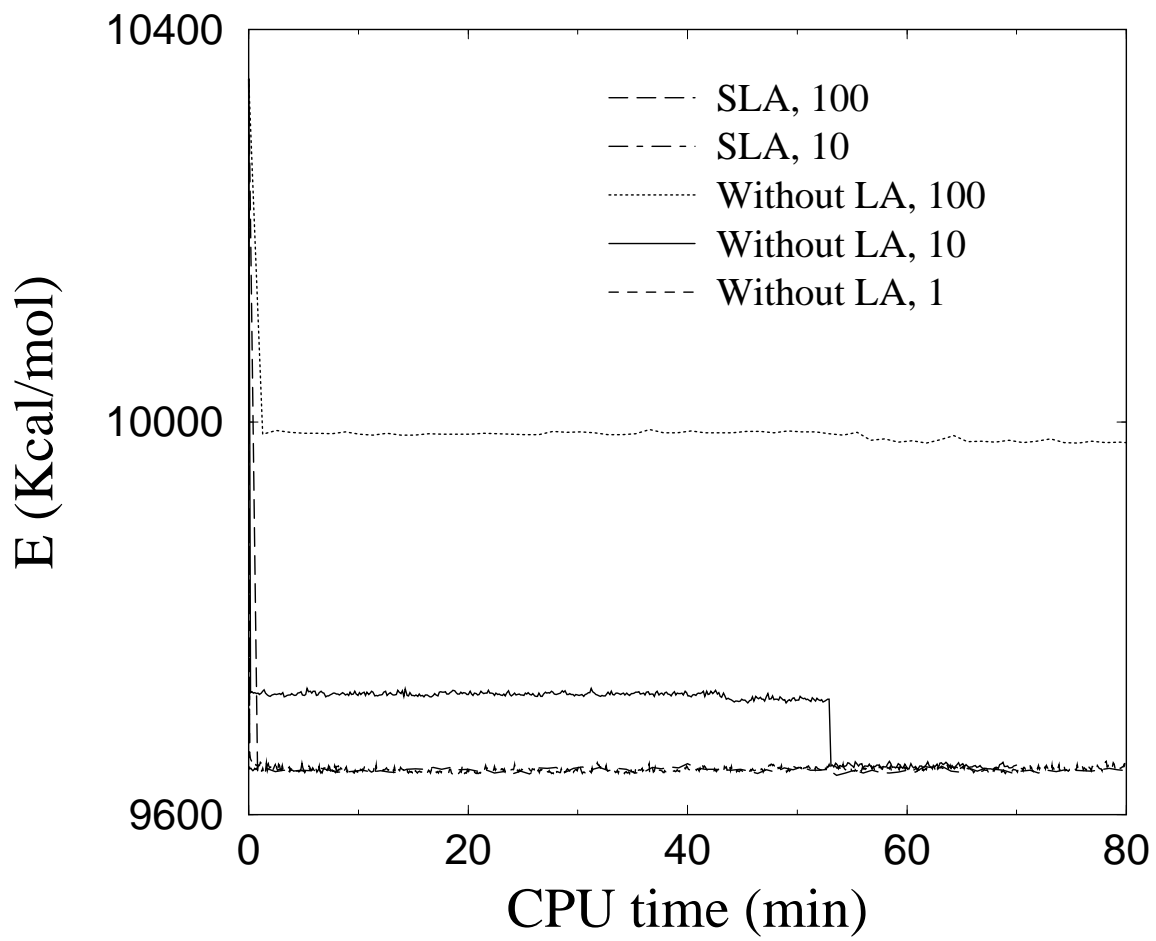


Figure 11: and Deem, 'Efficient Monte Carlo...'